INTERNATIONAL JOURNAL FOR NUMERICAL METHODS IN ENGINEERING
*Int. J. Numer. Meth. Engng* 2011; **87**:361–385
Published online 10 December 2010 in Wiley Online Library (wileyonlinelibrary.com). DOI: 10.1002/nme.3077

# Thermal coupling of fluid flow and structural response of a tunnel induced by fire

B. A. Schrefler[1], R. Codina[2], F. Pesavento[1,*,†] and J. Principe[2]

[1]*Department of Structural and Transportation Engineering, University of Padua, via Marzolo 9, 35131 Padova, Italy*
[2]*International Centre for Numerical Methods in Engineering—CIMNE, Universitat Politècnica de Catalunya, Edifici C-1, Campus Nord UPC, Gran Capitá, s/n, 08034 Barcelona, Spain*

SUMMARY

In this work we present the progress in the development of an algorithm for the simulation of thermal fluid–structural coupling in a tunnel fire. The coupling strategy is based on a Dirichlet/Neumann non-overlapping domain decomposition of the problem, which is carried out by developing a master code that controls solvers dedicated to the fluid mechanics and to the solid mechanics simulation. The computational fluid dynamics formulation consists of a stabilized finite element approximation of the low Mach number equations based on the subgrid scale concept, that allows us to deal with convection-dominated problems and to use equal order interpolation of velocity and pressure. The thermo-structural model of the tunnel vault, that considers a multiphase porous material where pores are partly filled with liquid and partly by gas, is specially devised for the simulation of concrete at high temperatures and consists of balance equations for mass conservation of dry air, mass conservation of water species (both in the liquid and gaseous state), enthalpy conservation and linear momentum conservation taking phase changes into account. The developed algorithm is applied to the problem of the response of a tunnel to a fire. We consider the combustion process as a heat release which can vary usually from 1 MW for small car fires to 100 MW for catastrophic fires. The released heat is transferred to the concrete walls of the tunnel which could cause extensive and heavy damage of the structure. Copyright © 2010 John Wiley & Sons, Ltd.

Received 25 February 2010; Revised 30 August 2010; Accepted 30 September 2010

KEY WORDS: coupling; fire; concrete; fluid–solid; computational fluid dynamics

## 1. INTRODUCTION

Fire in a tunnel is a catastrophic event which generally implies great risk for human beings, either users or fire brigades, and produces an important economic perturbation. In a first place because the closure of an infrastructure, such as a tunnel that connects two geographical regions that otherwise would be separated or reachable with difficulty, creates logistic problems. Transportation, in fact, is a key factor in modern economies and tunnels play a very crucial role in a continent like Europe, where the total length of these underground facilities exceeds 15 000 km [1]. In a second place because the action of a fire on the structure precludes further use of the tunnel unless extensive rebuilding is undertaken. The rehabilitation of the infrastructures requires an important economic effort to rebuild both the safety systems, the concrete structures, the pavement and all the necessary accessories, to permit again the circulation and the use of the tunnel.

*Correspondence to: F. Pesavento, Department of Structural and Transportation Engineering, University of Padua, via Marzolo 9, 35131 Padova, Italy.
†E-mail: pesa@dic.unipd.it, pesa@caronte.dic.unipd.it

After the most recent accidents that occurred in tunnels of the European road and rail networks, many related research projects have been started. Their aim is to cover the gap between the actual design standards, adopted so far to build underground facilities, and the new standards needed to ensure the safety also in the case of fire. A complete simulation of a fire in tunnel permits to have a deeper insight into the problem giving an important tool in order to define such standards. The interest in the problem considered here is demonstrated also by the large number of publications and European research projects. Another advantage of such a tool is to permit virtual training of fire brigade on real structure model to be ready for such an unfortunate event. Further the effects of improvements to enhance the fire resistance of the tunnel walls can be easily tested on a computer model.

A complete simulation of such a phenomenon is a complex task to solve which involves several engineering fields such as fluid dynamics, heat and mass transfer and structural behavior of concrete. Hence, more than one specialist has to be consulted to obtain a comprehensive evaluation of the problem. In these research projects, in fact, usually several Universities, Companies and Research Centers are involved, see e.g. the European project UPTUN [2].

The present work presents the progress in the development of an algorithm for the simulation of thermal fluid–structural coupling in a tunnel fire following the guidelines proposed in [3]. The model considers the fire as a source of heat, without taking into account the exact reactive mechanism as this would imply a precise knowledge of the chemical components of the fuel. The heat released during a fire, which is between 1 and 100 MW, is partially dissipated by the flow and partially transported toward the concrete structure where it is finally dissipated. Thus, the heat transfer involves both the behavior of the fluid inside tunnels and the structural behavior of the concrete. Although this simple model is used in this work, it should be mentioned that it would be important to consider the thermal radiation due to the strong influence it may have on the temperature distribution. If this phenomenon is taken into account it is also important to consider one of the products of the fire, the smoke, as it dramatically changes the radiative properties of the medium. This point is currently under development.

The model presented here is based on the solution of the thermal problem in the whole domain $\Omega$ that includes the structural domain $\Omega_S$ and the fluid domain $\Omega_F$, such that $\Omega = \Omega_S \cup \Omega_F$. The differential operators that describe the evolution of the temperature ($T$) are completely different in the two domains as a result of different physics and they depend on other variables that describe the state of each medium: the velocity ($\boldsymbol{v}$) and pressure ($p$) in the fluid and displacements ($\boldsymbol{u}$), gas pressure ($p^g$) and capillary pressure ($p^c$) in the structure. The mathematical model of each subproblem is presented in Section 2. The coupling appears on the interface conditions between the two subdomain as explained also in Section 2, where some approximations described in [4] are briefly revisited.

The numerical approximation to these problems, described in Section 3, is also different. The computational fluid dynamics formulation consists of a stabilized finite element approximation of the low Mach number equations based on the subgrid scale concept. Each field is decomposed into a resolvable and a subgrid scale part according to the finite element partition and the effect of the subgrid scale on the coarse scale is taken into account by an algebraic approximation. This approach allows us to deal with convection-dominated problems and to use equal order interpolation of velocity and pressure which would lead to numerical instabilities when a standard Galerkin formulation is used.

The numerical treatment of the structural problem requires the monolithic solution of four coupled differential equations the weak form of which is obtained by means of a weighted residual approach and the discretization is carried out by a Galerkin Finite Element approximation.

The coupling strategy was initially developed in [4] considering a solid with constant thermal properties (conductivity, density and specific heat). In this work it is extended to consider a solid with variable thermal properties which, in turn, depend on other state variables as described below. In our approach, each problem is solved using a different algorithm and in fact a different code. This is possible thanks to the implementation of the iteration by subdomain strategy to the Dirichlet/Neumann non-overlapping domain decomposition of the problem, which is based on the



DOI: 10.1002/nme

development of a relatively small master code. This code, developed following the MPI 2 standard, is in charge of managing the subdomain iterative coupling and the time marching loops. In this way, each dedicated code acts as a slave and can be updated separately as only minor modifications are needed to exchange the information with the master code.

The model is applied to the simulation of a fire in the Virgolo tunnel in Section 4. Finally, some conclusions are presented in Section 5 together with the proposal for future work.

## 2. PROBLEM DEFINITION

In this section we present the definition of the mathematical model. After presenting the mathematical model for the fluid dynamics and for the structural problems we briefly revisit the approximations to the interface conditions developed in [4] essential for the coupling strategy described in Section 3.

### *2.1. Fluid dynamics problem*

The equations that describe the dynamics of a compressible flow are the mass, momentum and energy conservation plus a state equation relating the thermodynamic variables. They read as

$$\frac{\mathrm{D}\rho}{\mathrm{D}t} = -\rho\nabla\cdot\boldsymbol{v},$$

$$\rho\frac{\mathrm{D}\boldsymbol{v}}{\mathrm{D}t} = \nabla\cdot\boldsymbol{\sigma}+\rho\boldsymbol{g},$$

$$\rho\frac{\mathrm{D}e}{\mathrm{D}t} = -\nabla\cdot\boldsymbol{q}+\boldsymbol{\sigma}:\varepsilon+q,$$

$$\rho = F(p,T).$$

Here, $\rho$ is the fluid density, $e$ is the internal energy, $\boldsymbol{g}$ and $q$ are the external force and energy source per unit of mass, respectively; $\boldsymbol{q}$ is the heat flux and $\boldsymbol{\sigma}$ the stress tensor related to the rate of deformation tensor (symmetric part of the velocity gradient, $\varepsilon(\boldsymbol{v})=\frac{1}{2}(\nabla\boldsymbol{v}+\nabla\boldsymbol{v}^{\mathrm{T}})$) through the following constitutive equations:

$$\boldsymbol{\sigma} = -p\boldsymbol{I}+2\mu\varepsilon'(\boldsymbol{v}),$$

$$\boldsymbol{q} = -k\nabla T,$$

where $k$ and $\mu$ are the conductivity and viscosity, $\boldsymbol{I}$ the identity tensor and $\varepsilon'(\boldsymbol{v})=\varepsilon(\boldsymbol{v})-\frac{1}{3}\nabla\cdot\boldsymbol{v}\boldsymbol{I}$ the deviatoric part of the rate of deformation tensor. The symbol $\mathrm{D}/\mathrm{D}t$ is used to denote the material time derivative.

In many cases of interest the flow can be considered as incompressible and this assumption is useful as it makes the problem much simpler than if a full compressible flow is considered. However, due to the presence of thermal effects, the flow cannot be considered as incompressible, although other approximations are possible [5]. A quite common one is the Boussinesq approximation that describes the thermal dependence of the flow by a linear relation between density and temperature. The validity of this approximation is restricted to the case of small temperature differences and cannot be used in the case of a fire. It is for this reason that the low Mach number approximation has been developed in the last 30 years. In this approximation the only assumption is that the Mach number of the flow is small, what leads to a splitting of the pressure in a constant-in-space thermodynamic part $p^{\mathrm{th}}$ that appears in the state equation and a mechanical part $p$ that appears in the momentum equation. This leads to a removal of the acoustic modes and the flow behaves as incompressible (in the sense that pressure is determined by the mass conservation equation and not by the state equation) but large variations of density due to temperature variations are allowed. This limit has been studied first in [6] in the inviscid case, and generalized to the viscous case



DOI: 10.1002/nme

in [7]. A rigorous derivation when combustion is also considered was presented in [8]. The low Mach number equations read as

$$\rho\frac{\partial \boldsymbol{v}}{\partial t}+\rho\boldsymbol{v}\cdot\nabla\boldsymbol{v}+\nabla p=\nabla\cdot(2\mu\varepsilon'(\boldsymbol{v}))+\rho\boldsymbol{g},$$

$$\frac{\partial \rho}{\partial t}+\nabla\cdot(\rho\boldsymbol{v})=0,$$

$$\rho c_{\mathrm{p}}\left(\frac{\partial T}{\partial t}+\boldsymbol{v}\cdot\nabla T\right)=\beta T\frac{\mathrm{d}p^{\mathrm{th}}}{\mathrm{d}t}+\nabla\cdot(k\nabla T)+q,$$

$$\rho=F(p^{\mathrm{th}},T).$$

Here, $\beta$ is the thermal expansion coefficient and $c_{\mathrm{p}}$ the constant pressure specific heat. The thermodynamic pressure $p^{\mathrm{th}}$ is constant over the whole domain and is determined from a global balance in the case of confined flows and is given by the external (atmospheric) pressure in the case of open flows [6]. The ideal gas law

$$\rho=\frac{p^{\mathrm{th}}}{RT}$$

is used as a state equation.

Another aspect that needs to be taken into account in this kind of problems is the turbulence modelling. Although the low Mach number equations fully describe the motion of the fluid, when the driving forces are strong the flow behavior is very complex and a detailed description of the movement would require a very fine discretization in order to accurately predict the flow evolution, which is not affordable in real scale problems. The traditional solution to this problem is to *modify the mathematical model* that describes the fluid motion to take into account these phenomena. The large eddy simulation (LES) of the flow is based on the filtering of the equations and results in the addition of a subgrid viscosity defined in terms of the velocity gradients. We follow this approach by means of the Smagorinsky model [9] in which the added viscosity is defined by

$$\mu_{\mathrm{LES}}=\rho c_{\mathrm{s}}\Delta^2[\varepsilon'(\boldsymbol{u}):\varepsilon'(\boldsymbol{u})]^{1/2},$$

where $c_{\mathrm{s}}$ is an empirical constant and $\Delta$ a characteristic length, usually taken as the mesh size. In an LES calculation, a subgrid thermal conductivity is also added. It is defined in terms of the subgrid viscosity as

$$k_{\mathrm{LES}}=\frac{\mu_{\mathrm{LES}}c_{\mathrm{p}}}{Pr^{\mathrm{T}}},$$

where $Pr^{\mathrm{T}}$ is the turbulent Prandtl number which is assumed to be constant (and taken to be 0.5). There is another approach to the solution of this problem that consists in *modifying the numerical approximation* of the equations to take into account these phenomena. It is based on the use of a stabilization technique, which is anyway needed to avoid numerical instabilities, conveniently modified to take into account non-linear phenomena. This possibility, which is currently under investigation will be mentioned in Section 3.

The motion of the fluid is driven by the external forces acting on it, which in the case of a fire in a tunnel are the gravity acceleration and the heat released by the fire. The definition of the flow problem is complete after the specification of boundary conditions. In the case of the velocity the non-slip condition is applied on the solid boundaries, the floor and tunnel walls. In the tunnel inlet the velocity can be prescribed to simulate a wind previous to the fire development or zero traction can be imposed. At the tunnel outlet zero traction is imposed. As far as the temperature field is concerned, zero heat flux is applied on the tunnel inlet and outlet. On the tunnel walls, temperature boundary conditions are responsible for the coupling of the structural problem and are discussed below.



DOI: 10.1002/nme

### 2.2. Structural problem

The thermo-structural model [10–13] considers concrete as multiphase porous material, where pores are partly filled with liquid water and partly with gas. The liquid phase consists of bound water and capillary or free water which appears when water content exceeds the solid saturation point. The gas phase is a mixture of dry air and water vapor. The set of balance equations for mass conservation of dry air, mass conservation of the water species, enthalpy conservation of the whole medium and linear momentum are solved to determine the state variables. This set is obtained neglecting inertia forces and convective heat flux related to the solid phase, eliminating the time derivative of the total porosity ($n$) by summing up equations of mass conservation of the fluids and mass conservation of solid phase and eliminating the mass source term due to phase change by summing up equations of mass conservation of liquid and vapor water. Its final form written at macroscopic level in terms of the primary variables ($p^{\mathrm{g}}$,$p^{\mathrm{c}}$, $T$, $\boldsymbol{u}$) and taking into account the small deformation theory, is:

- *Dry air mass balance equation* (including the solid skeleton mass balance) takes into account both diffusive and advective air flow, as well as variations of porosity caused by hydration process and deformations of the skeleton. It has the following form:

$$-n\frac{\mathrm{D}^{\mathrm{s}}S_{\mathrm{w}}}{\mathrm{D}t}-\beta_{\mathrm{s}}(1-n)S_{\mathrm{g}}\frac{\mathrm{D}^{\mathrm{s}}T}{\mathrm{D}t}+S_{\mathrm{g}}\nabla\cdot\boldsymbol{v}^{\mathrm{s}}+\frac{S_{\mathrm{g}}n}{\rho^{\mathrm{ga}}}\frac{\mathrm{D}^{\mathrm{s}}\rho^{\mathrm{ga}}}{\mathrm{D}t}+\frac{1}{\rho^{\mathrm{ga}}}\nabla\cdot\boldsymbol{J}_{\mathrm{g}}^{\mathrm{ga}}+\frac{1}{\rho^{\mathrm{ga}}}\nabla\cdot(nS_{\mathrm{g}}\rho^{\mathrm{ga}}\boldsymbol{v}^{\mathrm{gs}})$$
$$-\frac{(1-n)S_{\mathrm{g}}}{\rho^{\mathrm{s}}}\frac{\partial\rho^{\mathrm{s}}}{\partial\Gamma_{\mathrm{dehydr}}}\frac{\mathrm{D}^{\mathrm{s}}\Gamma_{\mathrm{dehydr}}}{\mathrm{D}t}=\frac{\dot{m}_{\mathrm{dehydr}}}{\rho^{\mathrm{s}}}S_{\mathrm{g}}, \tag{1}$$

  where $S_{\mathrm{w}}$ and $S_{\mathrm{g}}$ are the water and gas saturation level, respectively, $\beta_{\mathrm{s}}$ is the thermal expansion coefficient of the solid phase, $\rho^{\mathrm{ga}}$ is the dry air density, $\Gamma_{\mathrm{dehydr}}$ the hydration/dehydration degree, $\boldsymbol{J}_{\mathrm{g}}^{\mathrm{ga}}$ the dry air diffusive flux and $n$ the porosity. The terms on the right-hand side represent the source term related to the hydration ($\dot{m}_{\mathrm{hydr}}$). The operator $\mathrm{D}^{\mathrm{s}}/\mathrm{D}t$ is the material derivative with respect to the solid phase.
- *Water species* (*liquid+vapor*) *mass balance equation* (including the solid skeleton mass balance) considers diffusive and advective flow of water vapor, mass sources related to phase changes of vapor (evaporation–condensation, physical adsorption–desorption and dehydration), and variations of porosity caused by hydration/dehydration and leaching processes and deformations of the skeleton, resulting in the following equation:

$$n(\rho^{\mathrm{w}}-\rho^{\mathrm{gw}})\frac{\mathrm{D}^{\mathrm{s}}S_{\mathrm{w}}}{\mathrm{D}t}+(\rho^{\mathrm{w}}S_{\mathrm{w}}+\rho^{\mathrm{gw}}S_{\mathrm{g}})\alpha\nabla\cdot\boldsymbol{v}^{\mathrm{s}}-\beta_{swg}^{*}\frac{\mathrm{D}^{\mathrm{s}}T}{\mathrm{D}t}+S_{\mathrm{g}}n\frac{\mathrm{D}^{\mathrm{s}}\rho^{\mathrm{gw}}}{\mathrm{D}t}+\nabla\cdot\boldsymbol{J}_{\mathrm{g}}^{\mathrm{gw}}$$
$$+\nabla\cdot(n\,S_{\mathrm{w}}\rho^{\mathrm{w}}\boldsymbol{v}^{\mathrm{ls}})+\nabla\cdot(n\,S_{\mathrm{g}}\rho^{\mathrm{gw}}\boldsymbol{v}^{\mathrm{gs}})-(\rho^{\mathrm{w}}S_{\mathrm{w}}+\rho^{\mathrm{gw}}S_{\mathrm{g}})\frac{(1-n)}{\rho^{\mathrm{s}}}\left[\frac{\partial\rho^{\mathrm{s}}}{\partial\Gamma_{\mathrm{dehydr}}}\frac{\mathrm{D}^{\mathrm{s}}\Gamma_{\mathrm{dehydr}}}{\mathrm{D}t}\right]$$
$$=-\frac{\dot{m}_{\mathrm{dehydr}}}{\rho^{\mathrm{s}}}(\rho^{\mathrm{w}}S_{\mathrm{w}}+\rho^{\mathrm{gw}}S_{\mathrm{g}}-\rho^{\mathrm{s}}), \tag{2}$$

  where $\beta_{swg}^{*}=\beta_{\mathrm{s}}(1-n)(S_{\mathrm{g}}\rho^{\mathrm{gw}}+\rho^{\mathrm{w}}S_{\mathrm{w}})+n\,\beta_{\mathrm{w}}\rho^{\mathrm{w}}S_{\mathrm{w}}$ is the thermal expansion coefficient of the multiphase system, $\rho^{\mathrm{gw}}$ is the water vapor density and $\boldsymbol{J}_{\mathrm{g}}^{\mathrm{gw}}$ the water vapor diffusive flux.
- *Energy balance equation* (*for the whole system*) accounting for the conductive and convective heat flow, heat effects of phase changes and hydration/dehydration process, can be written as follows:

$$(\rho C_{\mathrm{p}})_{\mathrm{eff}}\frac{\partial T}{\partial t}+(\rho_{\mathrm{w}}C_{\mathrm{p}}^{\mathrm{w}}\boldsymbol{v}^{\mathrm{w}}+\rho_{\mathrm{g}}C_{\mathrm{p}}^{\mathrm{g}}\boldsymbol{v}^{\mathrm{g}})\cdot\nabla T-\nabla\cdot(\chi_{\mathrm{eff}}\nabla T)=-\dot{m}_{\mathrm{vap}}\Delta H_{\mathrm{vap}}-\dot{m}_{\mathrm{dehydr}}\Delta H_{\mathrm{dehydr}},$$



DOI: 10.1002/nme

where $\chi_{\text{eff}}$ is the effective conductivity from experiments, whereas the thermal capacity of the multiphase system and the enthalpy of vaporization and dehydration are, respectively:

$$\begin{aligned}(\rho C_{\text{p}})_{\text{eff}} &= \rho_{\text{s}} C_{\text{p}}^{\text{s}} + \rho_{\text{w}} C_{\text{p}}^{\text{w}} + \rho_{\text{g}} C_{\text{p}}^{\text{g}},\\ \Delta H_{\text{vap}} &= H^{\text{gw}} - H^{\text{w}},\\ \Delta H_{\text{dehydr}} &= H^{\text{ws}} - H^{\text{w}},\end{aligned} \tag{3}$$

with $\beta_{\text{sw}} = S_{\text{w}}[(1-n)\beta_{\text{s}} + n\beta_{\text{w}}]$.

- *Linear momentum balance equation* (*for the multiphase system*)

$$\nabla \cdot \boldsymbol{\sigma}^{\text{total}} + \rho \boldsymbol{g} = \boldsymbol{0}. \tag{4}$$

Here, $\rho$ is the solid density and $\boldsymbol{\sigma}^{\text{total}}$ is the total stress tensor in the sense of porous media mechanics and according to the 'effective stress principle' defined through Equation (5). In the Equations (1)–(4) the superscripts g, l and s indicate gas, liquid and solid phases, respectively, and a and w indicate the air and water vapor components of the gas phase. The liquid phase is bound water for $S \leqslant S_{\text{sp}}$ or capillary water for $S \geqslant S_{\text{sp}}$, where $S_{\text{sp}}$ is the solid saturation point. The total density is given by

$$\rho = (1-n)\rho^{\text{s}} + n S_{\text{w}} \rho^{\text{l}} + n(1-S_{\text{w}})\rho^{\text{g}}.$$

The densities of each component depend on the temperature and on the pressure, whereas the velocities of each phase relative to the solid skeleton depend on the pressure gradients and concentration of condensable and non-condensable species.

*2.2.1. Constitutive and state equations for description of chemo-hygro-thermal and mechanical state of concrete.* In the following the main constitutive relationships and state equations needed to close the model are briefly described for a sake of completeness. For a more detailed description the reader is referred to [11–14].

*Effective stress principle*: In the proposed approach concrete is treated as a multiphase porous material, so in the analysis of the stress state and the deformation of the material it is necessary to consider not only the action of an external load, but also the pressure exerted on the skeleton by fluids present in its voids. Hence, the total stress tensor $\boldsymbol{\sigma}^{\text{total}}$ acting in a point of the porous medium may be split into the effective stress $\eta^{\text{s}}\boldsymbol{\tau}^{\text{s}}$, which accounts for stress effects due to changes in porosity, spatial variation of porosity and the deformations of the solid matrix, and a part accounting for the solid phase pressure exerted by the pore fluids [15–18]

$$\eta^{\text{s}}\boldsymbol{\tau}^{\text{s}} = \boldsymbol{\sigma}^{\text{total}} + (p^{\text{g}} - x_{\text{s}}^{\text{ws}} p^{\text{c}})\boldsymbol{I}, \tag{5}$$

where $x_{\text{s}}^{\text{ws}}$ is the solid surface fraction in contact with the wetting film and $p^{\text{s}} = p^{\text{g}} - x_{\text{s}}^{\text{ws}} p^{\text{c}}$ is the so-called 'standard solid pressure' obtained in this form by neglecting the terms resulting from action of surface tension of solids on the interfaces with the pore fluids of the porous medium. This solid pressure form is related to the average normal stress exerted on the solid surface by the fluids $P^{\text{s}}$

$$P^{\text{s}} = -\langle \boldsymbol{n}_{\text{s}} \cdot \boldsymbol{\sigma}_{\text{s}} \cdot \boldsymbol{n}_{\text{s}} \rangle^{\text{ss}} \tag{6}$$

through the relationship $p^{\text{s}} = \alpha P^{\text{s}}$. In the last equation $\boldsymbol{\sigma}_{\text{s}}$ is the stress tensor of the solid phase at microscopic level, $\boldsymbol{n}_{\text{s}}$ is the unit vector normal to the solid phase in each point, while the Macaulay brackets $\langle\rangle^{\text{ss}}$ indicate an averaging over the solid surface. The coefficient $\alpha$ is the Biot constant that now can be interpreted as the the ratio of the hydrostatic part of the total stress tensor ($p^{\text{total}}$) to the normal force exerted on the solid surface by the surrounding fluids. For further details see [16–18].

*Dehydration process evolution law*, considering its irreversibility, has the form:

$$\Gamma_{\text{dehydr}}(t) = \Gamma_{\text{dehydr}}(T_{\max}(t)),$$



DOI: 10.1002/nme

thus

$$\dot{\Gamma}_{\text{dehydr}} = \frac{\partial \Gamma_{\text{dehydr}}(T)}{\partial T}\frac{\partial T}{\partial t} \quad \text{for } T(t) \geqslant T_{\max}(t),$$

$$\dot{\Gamma}_{\text{dehydr}} = 0 \quad \text{for } T(t) < T_{\max}(t),$$

where $T_{\max}(t)$ is the highest temperature reached by the concrete up to the time instant $t$. The constitutive relationship $\Gamma_{(\text{dehydr})}(T)$ can be obtained from the results of thermo-gravimetric (TG or DTA) tests, using the definition of the dehydration degree by means of the mass changes during concrete heating

$$\Gamma_{\text{dehydr}}(T) = \frac{m(T_0) - m(T)}{m(T_0) - m(T_\infty)},$$

where $m(T)$ is the mass of concrete specimen measured at temperature $T$ during TG tests, $T_0$ and $T_\infty$ are temperatures when the dehydration process starts and finishes. We assumed here $T_0 = 105^\circ\text{C}$ and $T_\infty = 1000^\circ\text{C}$.

*Thermo-chemical damage evolution equation*, obtained on the basis of the experimental results, takes into account the irreversible character of the material structural changes and may be written as [11]:

$$V(t) = V(T_{\max}(t)).$$

*Mechanical damage evolution equation*, of the following form:

$$d(t) = d(\tilde{\varepsilon}(t)) \tag{7}$$

is expressed in terms of the equivalent strain, $\tilde{\varepsilon}$, given by equations of the classical non-local, isotropic damage theory [19, 20]. The mechanical and thermo-chemical damage parameters, $d$ and $V$, are defined on basis of the experimentally determined stress-strain profiles at various temperatures, as follows [11]:

$$d = 1 - \frac{E(T)}{E_0(T)}; \quad V = 1 - \frac{E_0(T)}{E_0(T_a)}, \tag{8}$$

where the subscript '0' refers to the elastic behavior and $E(T)$ is the Young modulus at temperature $T$ different from the reference (i.e. ambient) temperature $T_a$. Taking into account a joint action of mechanical and thermo-chemical degradations, the total damage parameter, $D$ can be defined on the base of the following multiplicative combination [11]:

$$1 - D = \frac{E(T)}{E_0(T_a)} = \frac{E(T)}{E_0(T)}\frac{E_0(T)}{E_0(T_a)} = (1-d)\cdot(1-V). \tag{9}$$

Taking into account (7), (8), (5), the 'net' effective stress tensor $\eta^s\tilde{\boldsymbol{\tau}}^s$ (in the sense of damage mechanics) may be expressed as:

$$\eta^s\tilde{\boldsymbol{\tau}}^s = \frac{\boldsymbol{\sigma}^{\text{total}} + p^s\boldsymbol{I}}{(1-D)}, \tag{10}$$

where $p^s$ is the standard solid pressure defined previously. Thus, the linear momentum balance equation (4) has now the following form:

$$\boldsymbol{\nabla}\cdot(\eta^s\boldsymbol{\tau}^s - p^s\boldsymbol{I}) + \rho\boldsymbol{g} = 0.$$

By combining Equation (10) with the relation $\boldsymbol{\tau}^s = (1-D)\tilde{\boldsymbol{\tau}}^s$ the 'net' stress tensor is given by

$$\eta^s\boldsymbol{\tau}^s = (1-d)(1-V)\boldsymbol{\Lambda_0} : (\boldsymbol{\varepsilon}_{\text{tot}} - \boldsymbol{\varepsilon}_{\text{th}} - \boldsymbol{\varepsilon}_{\text{tchem}} - \boldsymbol{\varepsilon}_{\text{tr}}), \tag{11}$$

where $\boldsymbol{\Lambda_0}$ is the initial stiffness matrix and the tensors $\boldsymbol{\varepsilon}_{\text{th}}, \boldsymbol{\varepsilon}_{\text{tchem}}, \boldsymbol{\varepsilon}_{\text{tr}}$ are respectively the thermal strain, the thermo-chemical strain and the transient thermal strain which are defined in the following.



DOI: 10.1002/nme

The evolution equations shown above are not enough for a complete description of the material behavior. Indeed, an unloaded sample of plain concrete or cement stone, exposed for the first time to heating, exhibits considerable changes in its chemical composition, inner structure of porosity and changes in sample dimensions (irreversible in part). The concrete strains during first heating, called load-free thermal strains (LFTS) are usually treated as superposition of thermal and shrinkage components, and often are considered as almost inseparable. LFTS are decomposed into three main contributions [12]:

*Thermal dilatation strains*:

$$\mathrm{d}\boldsymbol{\varepsilon}_{\mathrm{th}} = \beta_{\mathrm{s}}(T)\,\mathrm{d}T.$$

*Capillary shrinkage strain*:

$$\mathrm{d}\boldsymbol{\varepsilon}_{\mathrm{sh}} = \frac{\alpha}{K_T}(\mathrm{d}x_{\mathrm{s}}^{\mathrm{ws}} p^{\mathrm{c}} + x_{\mathrm{s}}^{\mathrm{ws}} \mathrm{d}p^{\mathrm{c}})\boldsymbol{I},$$

where $K_T$ is the bulk modulus of the porous medium, and $\alpha$ is the Biot constant. This relationship is obtained according to the effective stress principle, Equation (5), and the definition of 'solid pressure' $p^{\mathrm{s}}$ given previously.

*Thermo-chemical strains*:

$$\mathrm{d}\boldsymbol{\varepsilon}_{\mathrm{tchem}} = \beta_{\mathrm{tchem}}(V)\,\mathrm{d}V,$$

where $\beta_{\mathrm{tchem}}(V) = \partial\boldsymbol{\varepsilon}_{\mathrm{tchem}}(V)/\partial V$ is obtained from experimental tests ($V$ is the thermo-chemical damage parameter).

As far as the first contribution is concerned, the strains are treated in a manner used in thermo-mechanics, but considering the thermal expansion coefficient $\beta_{\mathrm{s}}$ as a function of temperature. Shrinkage strains are modelled by means of the effective stress principle, in the form derived in Equation (5). For materials with very fine pores and well-developed internal pore surface, where water is also present as a thin film (like for example in concrete), the solid pressure relationship contains a coefficient $x_{\mathrm{s}}^{\mathrm{ws}}$, see Equation (5), instead of the classical saturation $S$ used in geomechanics [21]. This coefficient is a function of saturation $S$ and takes into account the disjoining pressure, which is important in the range of saturation in which only a thin film of water is adsorbed to the wall of the pores, see [12, 22] for details. In this way the contribution of the term related to the capillary pressure in Equation (5) can be interpreted as a sort of 'internal' load for the skeleton of the material. Hence, the associated shrinkage strains are not computed directly in the strain decomposition as it is usual in the classical phenomenological approaches but is already contained in the model. In heated concrete, above the temperature of about 105°C, the thermal decomposition of the cement matrix starts, and at higher temperatures also of aggregate (depending on its type and composition). This is a consequence of several complicated, endothermic chemical reactions, called concrete dehydration. As their result a considerable shrinkage of cement matrix (called chemical shrinkage) and usually expansion of aggregate are observed. Due to this contradictory behavior of the material components, cracks of various dimensions are developing when temperature increases, causing an additional change in concrete strains (usually expansion). These strains are modelled as function of thermo-chemical damage which takes into account the thermo-chemical deterioration of the material. During first heating, mechanically loaded concrete exhibits greater strains as compared to the load-free material at the same temperature. These additional deformations are referred to as load-induced thermal strains (LITS) [23]. A part of them originates just from the elastic deformation due to mechanical load, and it increases during heating because of thermo-chemical and mechanical degradation of the material strength properties. The time-dependent part of the strains during transient thermal processes due to temperature changes, is generally called thermal creep. Its physical nature is rather complicated and till now not fully understood, thus modelling is usually based on the results of special experimental tests. Typically, they are performed at constant heating rate equal to 2 K/min, for various (but constant during a particular test) levels of external load, $\sigma = \mathrm{const}$, ranging from 0% (load-free measurements) to 60% of the compressive strength of material at room temperature, $f_c(T_{\mathrm{a}})$. The formulation employed



DOI: 10.1002/nme

in the model is due to Thelandersson [24] in its original form, here modified using a coefficient $\bar{\beta}_{\mathrm{tr}}$ as a function of thermo-chemical damage $V$ and the effective stresses instead of total stresses, coupling in such a way the thermo-chemo-mechanical damage and capillary shrinkage model with the thermal creep model [12]:

$$\mathrm{d}\boldsymbol{\varepsilon}_{\mathrm{tr}} = \frac{\bar{\beta}_{\mathrm{tr}}}{f_c(T_{\mathrm{a}})}\boldsymbol{Q} : \eta^{\mathrm{s}}\tilde{\boldsymbol{\tau}}^{\mathrm{s}}\,\mathrm{d}V. \tag{12}$$

In Equation (12) $\boldsymbol{Q}$ is a fourth-order tensor that contains material parameters determined from transient thermal creep tests (the material is exposed to a temperature change under constant stress) [24], $\eta^{\mathrm{s}}\tilde{\boldsymbol{\tau}}^{\mathrm{s}}$ is the 'net' effective stress tensor and finally $f_c$ is the compressive strength of the material at 20°C. By considering rheological analogies, this corresponds to define an element of a Maxwell chain taking into account the thermo-mechanical interactions described above (i.e. the transient thermal strain).

The model in this form has been successfully used for solving several engineering problems, e.g. the case of fire in tunnels [3], spalling prediction [13] and in the simulation of different techniques for protecting concrete structures under fire [25].

### *2.3. Interface conditions*

To solve the thermo-mechanical problem on the domain $\Omega$ we consider a geometric domain decomposition of the problem by means of a non-overlapping subdomain approach. We split the domain into the fluid and structural subdomains as $\Omega = \Omega_{\mathrm{S}} \cup \Omega_{\mathrm{F}}$. The conditions to be satisfied at the interface are the continuity of the temperatures and velocities as well as the normal components of heat fluxes and tractions. If we denote by $\Gamma_{\mathrm{SF}}(t)$ the surface of the tunnel walls, these conditions read as

$$\begin{aligned}
\boldsymbol{v}_{\mathrm{F}}|_{\Gamma_{\mathrm{SF}}} &= \dot{\boldsymbol{u}}_{\mathrm{S}}|_{\Gamma_{\mathrm{SF}}},\\
\boldsymbol{n}\cdot\boldsymbol{\sigma}_{\mathrm{F}}|_{\Gamma_{\mathrm{SF}}} &= \boldsymbol{n}\cdot\boldsymbol{\sigma}_{\mathrm{S}}|_{\Gamma_{\mathrm{SF}}},\\
T_{\mathrm{F}}|_{\Gamma_{\mathrm{SF}}} &= T_{\mathrm{S}}|_{\Gamma_{\mathrm{SF}}},\\
\boldsymbol{n}\cdot\boldsymbol{q}_{\mathrm{F}}|_{\Gamma_{\mathrm{SF}}} &= \boldsymbol{n}\cdot\boldsymbol{q}_{\mathrm{S}}|_{\Gamma_{\mathrm{SF}}},
\end{aligned}$$

where it is explicitly noted that $\Gamma_{\mathrm{SF}}(t)$ is actually a moving surface and its position depends on the solution of the structural problem. The approximations proposed in [4] are based on two assumptions

1. *The velocities and the displacements of the solid medium are small* (*compared to the dimensions of the tunnel*).
2. *The mechanical traction produced by the fluid on the solid is small.*

These assumptions result in $\dot{\boldsymbol{u}}_{\mathrm{S}} \approx \boldsymbol{0}$ and $\boldsymbol{n}_{\mathrm{F}}\cdot\boldsymbol{\sigma}_{\mathrm{F}}|_{\Gamma_{\mathrm{SF}}} \approx \boldsymbol{0}$ and therefore the boundary $\Gamma_{\mathrm{SF}}(t)$ remains fixed and the interface conditions become

$$\begin{aligned}
\boldsymbol{v}_{\mathrm{F}}|_{\Gamma_{\mathrm{SF}}} &= \boldsymbol{0},\\
\boldsymbol{n}\cdot\boldsymbol{\sigma}_{\mathrm{S}}|_{\Gamma_{\mathrm{SF}}} &= \boldsymbol{0},\\
T_{\mathrm{F}}|_{\Gamma_{\mathrm{SF}}} &= T_{\mathrm{S}}|_{\Gamma_{\mathrm{SF}}},\\
\boldsymbol{n}\cdot\boldsymbol{q}_{\mathrm{F}}|_{\Gamma_{\mathrm{SF}}} &= \boldsymbol{n}\cdot\boldsymbol{q}_{\mathrm{S}}|_{\Gamma_{\mathrm{SF}}}.
\end{aligned}$$

Thus, the coupling between the solid and the fluid is due to the thermal problem only.

A further approximation was developed in [4] to consider the problem of the strong boundary layers present in a turbulent flow. This second approximation is based on a non-overlapping domain decomposition of the problem in three subdomains, one in the solid region and two in the fluid region. One of the fluid subdomains will be a thin region of thickness $\delta$ near the solid surface and the other will be the rest of the fluid domain. Using the well-known wall function approach [9], the



DOI: 10.1002/nme

problem in boundary layer is approximately solved and an iteration strategy between the remaining subdomains is proposed. Therefore, this second approach also involves two subdomains but the interface conditions now read as

$$\boldsymbol{t}|_{\Gamma_{SF}} = \gamma \boldsymbol{v}_F|_{\Gamma_{SF}},$$

$$\boldsymbol{n}_F \cdot \boldsymbol{v}_F|_{\Gamma_{SF}} = 0,$$

$$\boldsymbol{n}_S \cdot \boldsymbol{\sigma}_S|_{\Gamma_{SF}} = \boldsymbol{0}$$

and

$$\boldsymbol{n}_S \cdot \boldsymbol{q}_S|_{\Gamma_{SF}} = -\boldsymbol{n}_F \cdot \boldsymbol{q}_F|_{\Gamma_{SF}} = \alpha_c (T_F|_{\Gamma_{SF}} - T_S|_{\Gamma_{SF}}), \tag{13}$$

where $\boldsymbol{t}$ is now the tangential stress acting on the fluid

$$\boldsymbol{t} = [\boldsymbol{n} \cdot \boldsymbol{\sigma}_F - (\boldsymbol{n} \cdot \boldsymbol{\sigma}_F \cdot \boldsymbol{n})\boldsymbol{n}]_{\Gamma_{SF}}$$

and $\gamma$ and $\alpha_c$ are parameters that depend on the wall function coefficients. The first one is computed from the universal velocity profile assumed in the wall function approach, as usual [9]. The second could also be computed in a similar fashion but it is estimated from experimental values in this work. It is also important to remark that we do not consider any mass exchange between the solid and the fluid. Even if the structural model is dependent on the mass loss coefficient $\beta_c$ we do not take into account the corresponding change of mass in the fluid. The influence of choice of $\alpha_c$ and $\beta_c$ is shown in Section 4.

## 3. NUMERICAL APPROXIMATION

In this section we present the numerical approximation to the problem and some details of the implementation are carried out.

### *3.1. Fluid dynamics problem*

The numerical approximation of the fluid dynamics problem has been presented in [26] and is briefly described here. The low Mach number equations presented in Section 2 can be written as a system of non-linear convection–diffusion–reaction equations of the form

$$\mathscr{L}(\boldsymbol{U}; \boldsymbol{U}) := \boldsymbol{M}(\boldsymbol{U}) \frac{\partial \boldsymbol{U}}{\partial t} + \boldsymbol{A}_i(\boldsymbol{U}) \frac{\partial \boldsymbol{U}}{\partial x_i} - \frac{\partial}{\partial x_i} \left( \boldsymbol{K}_{ij} \frac{\partial \boldsymbol{U}}{\partial x_j} \right) + \boldsymbol{S}(\boldsymbol{U}) \boldsymbol{U} = \boldsymbol{F}, \tag{14}$$

where $\boldsymbol{U} = (\boldsymbol{u}, p, T)$ is the unknown vector of size $n_{unk} = n_{sd} + 2$, $\boldsymbol{F}$ is a given vector of size $n_{unk}$, $\boldsymbol{A}_i$, $\boldsymbol{K}_{ij}$ and $\boldsymbol{S}$ are matrices of size $n_{unk} \times n_{unk}$ ($i, j = 1, ..., n_{sd}$) whose expressions for the low Mach number equations are given in [26] and for the Navier–Stokes equations in [27, 28], $n_{unk}$ is the number of unknowns of the problem and $n_{sd}$ is the number of space dimensions. Just to simplify the presentation of the stabilized formulation, let us consider the simple case in which Dirichlet boundary conditions are imposed on $\partial\Omega$ and a steady-state problem. In such a case, if $\mathscr{W}$ is the functional space where the solution is to be sought (the components of $\boldsymbol{u}$ and $T$ must be $H^1(\Omega)$ functions satisfying the Dirichlet boundary conditions, whereas $p$ must be a $L^2(\Omega)/\Re$ function) and $\mathscr{W}_0$ denotes the corresponding space of test functions, the weak form of the problem consists in finding $\boldsymbol{U} \in \mathscr{W}$ such that

$$B(\boldsymbol{U}; \boldsymbol{U}, \boldsymbol{V}) - L(\boldsymbol{V}) = 0 \quad \forall \boldsymbol{V} \in \mathscr{W}_0, \tag{15}$$

where the non-linear form $B$ and the linear form $L$ are defined as

$$B(\boldsymbol{U}_0; \boldsymbol{U}, \boldsymbol{V}) := \langle \boldsymbol{V}^t, \mathscr{L}(\boldsymbol{U}_0; \boldsymbol{U}) \rangle := \int_\Omega \boldsymbol{V}^t \boldsymbol{A}_i(\boldsymbol{U}_0) \frac{\partial \boldsymbol{U}}{\partial x_i} + \int_\Omega \frac{\partial \boldsymbol{V}^t}{\partial x_i} \boldsymbol{K}_{ij} \frac{\partial \boldsymbol{U}}{\partial x_j} + \int_\Omega \boldsymbol{V}^t \boldsymbol{S}(\boldsymbol{U}_0) \boldsymbol{U},$$

$$L(V) := \int_\Omega \boldsymbol{V}^t \boldsymbol{F}.$$



DOI: 10.1002/nme

The Galerkin finite element approximation of this problem is standard. Based on a partition of the domain $\mathscr{P}_h=\{K\}$ in $n_{\mathrm{el}}$ elements $K$, the space $\mathscr{W}$ is approximated by a finite dimensional space $\mathscr{W}_h$ (built using polynomials). If the space of test functions $\mathscr{W}_0$ is approximated by $\mathscr{W}_{0,h}$, defined in a similar way, the discrete problem consists in finding $\boldsymbol{U}_h\in\mathscr{W}_h$ such that

$$B(\boldsymbol{U}_h;\boldsymbol{U}_h,\boldsymbol{V}_h)-L(\boldsymbol{V}_h)=0\quad\forall\boldsymbol{V}_h\in\mathscr{W}_{0,h}.$$

It is well known that this formulation lacks stability when the diffusive terms are small, compared either with the convective or with the reactive terms. Likewise, since the quadratic form associated to $\boldsymbol{K}_{ij}$ is not positive definite, it is not possible to use equal interpolation for all the components of $\boldsymbol{U}$. In our case, velocity–pressure pairs must satisfy the inf–sup condition. If the thermal coupling is strong, this could also lead to a source of numerical instabilities.

The stabilized finite element formulation we employ to solve problem (15) is based on the subgrid scale method with an algebraic approximation to the subscales [29]. Let us consider for the moment a linearized version of the problem of the form

$$B(\boldsymbol{U}_{0,h};\boldsymbol{U},\boldsymbol{V})-L(\boldsymbol{V})=0\quad\forall\boldsymbol{V}\in\mathscr{W}_0,$$

where $\boldsymbol{U}_{0,h}$ is a known finite element function. We will not detail here the derivation of the method, for which the reader is referred to [26]. The subgrid scale method is based on a decomposition of the space of the form

$$\mathscr{W}=\mathscr{W}_h\oplus\widetilde{\mathscr{W}},$$

where $\widetilde{\mathscr{W}}$ can be in principle any space to complete $\mathscr{W}_h$ in $\mathscr{W}$. To fix ideas, we may think of $\widetilde{\mathscr{W}}$ as the orthogonal complement of $\mathscr{W}_h$ with respect to the $L^2$ inner product in $\mathscr{W}$. Since $\widetilde{\mathscr{W}}$ represents the component of $\mathscr{W}$ which is not reproduced by the finite element space, we call it the space of subscales or subgrid scales. The continuous equation (15) can now be written as the system

$$B(\boldsymbol{U}_{0,h};\boldsymbol{U}_h,\boldsymbol{V}_h)+B(\boldsymbol{U}_{0,h};\widetilde{\boldsymbol{U}},\boldsymbol{V}_h)=L(\boldsymbol{V}_h)\quad\forall\boldsymbol{V}_h\in\mathscr{W}_h,\tag{16}$$

$$B(\boldsymbol{U}_{0,h};\boldsymbol{U}_h,\widetilde{\boldsymbol{V}})+B(\boldsymbol{U}_{0,h};\widetilde{\boldsymbol{U}},\widetilde{\boldsymbol{V}})=L(\widetilde{\boldsymbol{V}})\quad\forall\widetilde{\boldsymbol{V}}\in\widetilde{\mathscr{W}},\tag{17}$$

where $\boldsymbol{U}=\boldsymbol{U}_h+\widetilde{\boldsymbol{U}}$ and $\boldsymbol{U}_h\in\mathscr{W}_h$,$\widetilde{\boldsymbol{U}}\in\widetilde{\mathscr{W}}$.

The final discrete weak form of the problem reads as: find $\boldsymbol{U}_h\in\mathscr{W}_h$ such that

$$B(\boldsymbol{U}_{0,h};\boldsymbol{U}_h,\boldsymbol{V}_h)+\int_{\Omega'}\widetilde{\boldsymbol{U}}^t\mathscr{L}^*(\boldsymbol{U}_{0,h};\boldsymbol{V}_h)=L(\boldsymbol{V}_h),$$

where $\mathscr{L}^*$ is the adjoint operator of $\mathscr{L}$ with homogeneous Dirichlet conditions and $\widetilde{\boldsymbol{U}}$ is given by (18), and the so-called *subgrid scales* are given by

$$\widetilde{\boldsymbol{U}}\approx\boldsymbol{\tau}[\boldsymbol{F}-\mathscr{L}(\boldsymbol{U}_{0,h};\boldsymbol{U}_h)].\tag{18}$$

The way to compute matrix $\boldsymbol{\tau}$ in general situations is still not clear. Traditionally, the way to proceed has been to obtain particular expressions for simplified problems and then to extend them to more complex situations. Very often, the appropriateness of the expressions thus obtained has been confirmed by convergence analysis. A simple approximation for $\boldsymbol{\tau}$ [30] that we will use here is given (in the two-dimensional case) by

$$\boldsymbol{\tau}=\mathrm{diag}(\tau_1,\tau_1,\tau_2,\tau_3),$$

where

$$\tau_1=\left[c_1\frac{\mu}{h^2}+c_2\frac{\rho|\boldsymbol{u}_{0,h}|}{h}\right]^{-1},\quad\tau_2=\frac{h^2}{c_1\tau_1},\quad\tau_3=\left[c_1\frac{k}{h^2}+c_2\frac{\rho|\boldsymbol{u}_{0,h}|}{h}\right],$$

where $c_1$ and $c_2$ are algorithmic constants that we take $c_1=4$ and $c_2=2$ for linear elements and $\boldsymbol{u}_{0,h}$ is the velocity component of $\boldsymbol{U}_{0,h}$.



DOI: 10.1002/nme

Concerning the time integration, we use the generalized trapezoidal rule. In particular, the second-order Crank–Nicolson scheme is used for the numerical example to be presented in Section 4. A fixed point method is used as linearization scheme. For brevity, only the time integration and linearization for the structural problem will be detailed.

The possibility of modifying this formulation to take turbulence into account is based on the idea of tracking the subscales. This idea, introduced in [30] consist in following the evolution the subscales in time as well as along the non-linear iteration. This implies in particular that $\boldsymbol{U}_{0,h}$ should be really taken to be $\boldsymbol{U}_{0,h}+\widetilde{\boldsymbol{U}}$ but as the subgrid scale depends on the residual, it is necessary to store the value calculated at the previous non-linear iteration. This approach leads to a formulation that takes into account all the non-linear terms as it is done in LES giving the possibility of *using the stabilized formulation as a turbulence model*. This possibility is, however, under investigation (see [31] for some ideas in this direction).

### *3.2. Structural problem*

The weak form of the governing equations of the model are obtained by weighted residual approach. These equations are then discretised in space by means of a Galerkin finite element approximation [32]. The unknown variables are expressed in terms of their nodal values as

$$p^{\mathrm{g}}(t)\cong \boldsymbol{N}_{\mathrm{p}}\bar{\boldsymbol{p}}^{\mathrm{g}}(t),\quad p^{\mathrm{c}}(t)\cong \boldsymbol{N}_{\mathrm{p}}\bar{\boldsymbol{p}}^{c}(t),$$

$$T(t)\cong \boldsymbol{N}_{t}\bar{\boldsymbol{T}}(t),\quad \boldsymbol{u}(t)\cong \boldsymbol{N}_{u}\bar{\boldsymbol{u}}(t),$$

where $\boldsymbol{N}_{\mathrm{p}}$, $\boldsymbol{N}_{t}$ and $\boldsymbol{N}_{u}$ are the shape function matrices. As well known in poro-elastic problems different order shape functions for displacements and pressures are usually needed to obtain a stable solution in the region close to full saturation, but here we deal with a partially saturated material far from the incompressibility condition hence the same shape functions can be used for all the state variables. Likewise, advective terms in Equations (1) and (2) are not dominant and therefore there is no need of using stabilization techniques as those described in the previous subsection. Therefore, the variational or weak form of the model equations was obtained in [11] by means of Galerkin's method (weighted residuals), and after application of Green's theorem, it can be written in the following concise matrix form:

$$\boldsymbol{C}(\bar{\boldsymbol{x}})\frac{\partial\bar{\boldsymbol{x}}}{\partial t}+\boldsymbol{K}(\bar{\boldsymbol{x}})\bar{\boldsymbol{x}}=\boldsymbol{f}(\bar{\boldsymbol{x}}),$$

with

$$\boldsymbol{C}=\begin{bmatrix}\boldsymbol{C}_{gg} & \boldsymbol{C}_{gc} & \boldsymbol{C}_{gt} & \boldsymbol{C}_{gu}\\ \boldsymbol{0} & \boldsymbol{C}_{cc} & \boldsymbol{C}_{ct} & \boldsymbol{C}_{cu}\\ \boldsymbol{0} & \boldsymbol{C}_{tc} & \boldsymbol{C}_{tt} & \boldsymbol{C}_{tu}\\ \boldsymbol{0} & \boldsymbol{0} & \boldsymbol{0} & \boldsymbol{0}\end{bmatrix},\quad \bar{\boldsymbol{x}}=\begin{Bmatrix}\bar{\boldsymbol{p}}^{\mathrm{g}}\\ \bar{\boldsymbol{p}}^{c}\\ \bar{\boldsymbol{T}}\\ \bar{\boldsymbol{u}}\end{Bmatrix},$$

$$\boldsymbol{K}=\begin{bmatrix}\boldsymbol{K}_{gg} & \boldsymbol{K}_{gc} & \boldsymbol{K}_{gt} & \boldsymbol{0}\\ \boldsymbol{K}_{cg} & \boldsymbol{K}_{cc} & \boldsymbol{K}_{ct} & \boldsymbol{0}\\ \boldsymbol{K}_{tg} & \boldsymbol{K}_{tc} & \boldsymbol{K}_{tt} & \boldsymbol{0}\\ \boldsymbol{K}_{ug} & \boldsymbol{K}_{uc} & \boldsymbol{K}_{ut} & \boldsymbol{K}_{uu}\end{bmatrix},\quad \boldsymbol{f}=\begin{Bmatrix}\boldsymbol{f}_{\mathrm{g}}\\ \boldsymbol{f}_{c}\\ \boldsymbol{f}_{t}\\ \boldsymbol{f}_{u}\end{Bmatrix},$$

where $\bar{\boldsymbol{x}}$ is the vector of nodal values of state variables, and the non-linear matrix coefficients $\boldsymbol{C}(\bar{\boldsymbol{x}})$, $\boldsymbol{K}(\bar{\boldsymbol{x}})$ and $\boldsymbol{f}(\bar{\boldsymbol{x}})$ are defined in detail in [13, 33]. The time discretization is accomplished through a fully implicit finite difference scheme (backward difference),

$$\boldsymbol{\Psi}(\bar{\boldsymbol{x}}^{n+1})=\boldsymbol{C}(\bar{\boldsymbol{x}}^{n+1})\frac{\bar{\boldsymbol{x}}^{n+1}-\bar{\boldsymbol{x}}^{n}}{\Delta t}+\boldsymbol{K}(\bar{\boldsymbol{x}}^{n+1})\bar{\boldsymbol{x}}^{n+1}-\boldsymbol{f}(\bar{\boldsymbol{x}}^{n+1})=\boldsymbol{0},$$



DOI: 10.1002/nme

where the superscript $n$ is the time step number and $\Delta t$ the time step length. The above equation set is solved by means of a monolithic Newton–Raphson-type iterative procedure [11]:

$$\boldsymbol{\Psi}((\bar{\boldsymbol{x}}^{n+1})^k) = -\left.\frac{\boldsymbol{\Psi}(\boldsymbol{x})}{\partial \boldsymbol{x}}\right|_{(\bar{\boldsymbol{x}}^{n+1})^k} (\Delta \bar{\boldsymbol{x}}^{n+1})^k,$$

$$(\bar{\boldsymbol{x}}^{n+1})^{k+1} = (\bar{\boldsymbol{x}}^{n+1})^k + (\Delta \bar{\boldsymbol{x}}^{n+1})^k,$$

where $k$ is the iteration index and

$$\frac{\partial \boldsymbol{\Psi}(\boldsymbol{x})}{\partial \boldsymbol{x}}$$

is the Jacobian matrix. A two-stage solution strategy has been applied at every time step to take into account damage of concrete. First an intermediate problem, keeping the mechanical damage value constant and equal to that obtained at the previous time step, is solved. Then, the 'final' solution is obtained, for all state variables and total damage parameter, by means of the modified Newton–Raphson method, using the tangential or Jacobian matrix from the last iteration of the first stage. This allowed us to avoid differentiation with respect to the damage and to obtain a converging solution [11].

### *3.3. Coupling strategy*

As mentioned before we consider a geometric domain decomposition of the problem by means of a non-overlapping subdomain approach. Therefore, we expect to construct the problem solution from the solution of local problems for the fluid and the structure using the interface conditions already described. This is carried out by iteratively solving local problems on each domain until convergence on the interface conditions is satisfied that is to say, we use an iteration-by-subdomain strategy. If $\mathscr{L}$ denotes the differential operator on the domain and $\mathscr{B}$ the differential operator on the boundary the situation is as follows. On the fluid region we solve at the iteration $i$ of each time step:

$$\mathscr{L}_{\mathrm{F}}(T_{\mathrm{F}}^i) = f_{\mathrm{F}} \quad \text{in } \Omega_{\mathrm{F}},$$

$$\mathscr{B}_{\mathrm{F}}(T_{\mathrm{F}}^i) = g_{\mathrm{F}} \quad \text{in } \partial\Omega_{\mathrm{F}} - \Gamma_{\mathrm{SF}},$$

$$\mathscr{B}_{\mathrm{FS}}(T_{\mathrm{F}}^i) = \mathscr{B}_{\mathrm{FS}}(T_{\mathrm{S}}^{i-1}) \quad \text{in } \Gamma_{\mathrm{SF}},$$

where boundary conditions on $\Gamma_{\mathrm{SF}}$ depend on the solution of the structural problem at the previous iteration. On the structural domain we solve at the $i$th iteration

$$\mathscr{L}_{\mathrm{S}}(T_{\mathrm{S}}^i) = f_{\mathrm{S}} \quad \text{in } \Omega_{\mathrm{S}},$$

$$\mathscr{B}_{\mathrm{S}}(T_{\mathrm{S}}^i) = g_{\mathrm{F}} \quad \text{in } \partial\Omega_{\mathrm{S}} - \Gamma_{\mathrm{SF}},$$

$$\mathscr{B}_{\mathrm{SF}}(T_{\mathrm{S}}^i) = \mathscr{B}_{\mathrm{SF}}(T_{\mathrm{F}}^k) \quad \text{in } \Gamma_{\mathrm{SF}},$$

where we can take $k = i$ or $k = i - 1$. In the first case the solution of this problems is sequential whereas in the second one it can be parallel. The choice of the boundary conditions of the local problems should be such that interface conditions presented in Section 2 are satisfied when convergence is achieved. It is well known from the theory of domain decomposition methods that in the case of non-overlapping subdomains we can choose Dirichlet–Neumann(Robin); Neumann(Robin)–Dirichlet or Robin–Robin conditions. In this work we apply the interface conditions described in Section 2.3.

One important point of this strategy is that we already have programs that solve the fluid dynamics problem and the structural problem. Then a master/slave algorithm was implemented by developing a third code (the master code) in order to control the iterative process. The MPICH2 library, an implementation of the MPI-2 standard, provides functions for process communications



DOI: 10.1002/nme

that are used to interchange the data needed to apply boundary conditions on each dedicated (slave) code. Some minor modifications on these codes are needed in order to exchange data with the master. In order to perform a calculation, input data for each subproblem need to be generated and the master code starts the calculation by starting the slave process (this is only possible under MPI-2 standard). During the calculation the master code needs to define the boundary conditions to be applied on each subproblem.

A particular aspect of this implementation is the need of coupling a two-dimensional code with a three-dimensional one. On the one hand, due to the high number of state variables of the structural model, only two-dimensional calculations are performed using the structural code. On the other hand, three-dimensional calculations can be performed using the fluid dynamics code. Therefore, the three-dimensional concrete tunnel vault is approximated by several two-dimensional sections and variables are linearly interpolated to generate boundary conditions on the fluid. This task is also performed by the master code. The values of the temperature or heat flux to be applied as boundary condition on an interface node need to be calculated from the temperature on the other subdomain. This is done by finding the host element and interpolating. The element search strategy used is based on the quad-tree algorithm.

## 4. NUMERICAL APPLICATIONS

The models presented in Section 2 have been applied to the analysis of behavior of concrete tunnel in the event of fire.

Under severe conditions in terms of temperature and pressure, concrete structures experience spalling, which results in rapid loss of the surface layers of the concrete at temperature exceeding about 200–300°C. As a result, the core concrete is exposed to these temperatures, thereby increasing the rate of heat transmission to the core part of the element and in particular to the reinforcement, what may pose a risk for the integrity of the concrete structure.

It is commonly believed that the main reasons of the thermal spalling are: build-up of high pore pressure close to the heated concrete surface as a result of rapid evaporation of moisture, and the release of the stored energy due to the thermal stresses resulting from high values of restrained strains caused by temperature gradients. Nevertheless, relative importance of the two mechanisms is not established yet and still needs further studies, both experimental and theoretical. The results of the research performed till now show that the fire performance of concrete structures is influenced by several factors, such as initial moisture content of the concrete, the rate of temperature increase (fire intensity), porosity (density) and permeability of the concrete, its compressive strength, type of aggregate, dimensions and shape of a structure, its lateral reinforcement and loading conditions. Hence, it is important to use a thermo-structural model that takes into account the global thermo-chemo-hygro-mechanical behavior of the material similar to the one presented in Section 2.2. Its coupling with the fluid dynamics model allows for a realistic simulation of fire scenario. Indeed, the accidents due to fires, occurred in major European tunnels in the last 15 years (Channel, Mont-Blanc, Great Belt Link, Tauern) have shown that the duration of the fire was longer than expected and the produced temperature fields were much more severe than those considered in standard codes. Moreover, the post-inspection showed extensive and heavy damage in the concrete elements which, in the case of the Mont-Blanc fire, seriously compromised the access of the firemen to the fire place.

In the following the results of some numerical computations obtained by applying the coupled tool described in the previous sections are shown. The structure under consideration is the tunnel of Virgolo close to Bolzano (Italy) that has been also used for an experimental test in the framework of UPTUN project [2]. We have considered the central part of the tunnel, 80 m long. Its geometry is decomposed into the fluid and the solid domains, see Figures 1–3. The solid domain consists in the cross-section of the tunnel vault. In the simulations five cross-sections are considered at 0, 30, 40, 50, 80 m along the longitudinal axis $z$. The section at 40 m is the location of fire. The fluid is considered as an ideal gas and has the following properties: dynamic viscosity $\mu = 1.8^{-5}\,\mathrm{kg/(ms)}$, specific heat



DOI: 10.1002/nme

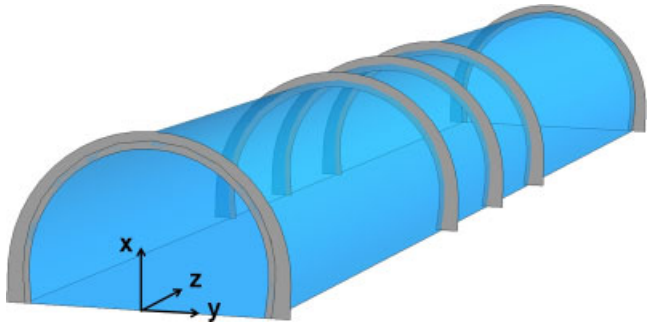


Figure 1. Global geometry of the tunnel.

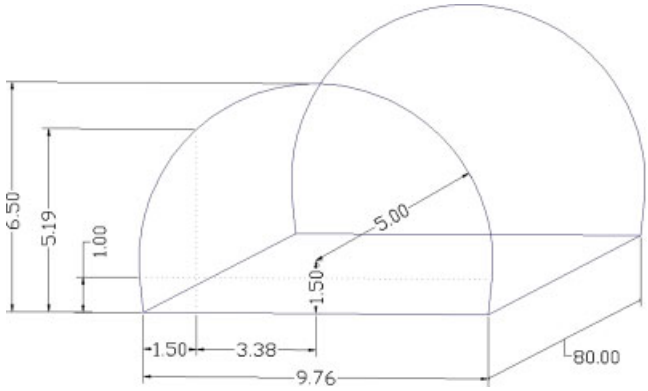


Figure 2. Geometry of the 3D fluid domain.

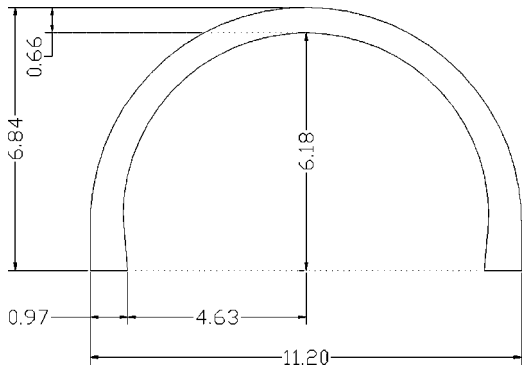


Figure 3. Geometry of the tunnel cross-section (solid domain).

$c_p = 1006.0\,\mathrm{J/(kg\,K)}$, thermal conductivity $\lambda_f = 0.026\,\mathrm{W/(mK)}$, density $\rho = 1.225\,\mathrm{kg/m^3}$. Concrete used for the solid domain (i.e. the sections of the concrete tunnel) is C60 concrete (with a final compressive strength equal to 60 MPa) and has the following main properties at ambient temperature (20°C): elastic modulus $E = 40\,000\,\mathrm{MPa}$, porosity $n = 0.082$, intrinsic permeability $k = 2 \times 10^{-18}\,\mathrm{m^2}$, solid density $\rho_s = 2564\,\mathrm{kg/m^3}$, solid thermal conductivity $\lambda_s = 1.92\,\mathrm{W/(mK)}$, solid specific heat $c_{ps} = 855.52\,\mathrm{J/(kg\,K)}$. The volumetric heat source corresponding to the fire is located at the coordinates $(x, y, z) = (1.0, 0.5, 40.0)$ and has a volume equal to $8\,\mathrm{m^3}$. This means that the fire is located in the central section of the tunnel at 0.5 m from the longitudinal axis and at 1 m height from the road pavement.



DOI: 10.1002/nme

Five different cases are considered in the computations:

1. fire with a total thermal power equal to 10 MW (fire duration: 10 min) which is indicated hereafter as the 'standard case';
2. fire with a total thermal power equal to 20 MW (fire duration 60 min) which is indicated hereafter as the 'real case';
3. sensitivity analysis of the heat and mass exchange coefficients $\alpha_c$, $\beta_c$. The latter parameter governs the water vapor mass exchange between the heated surface of the concrete structure and the surrounding environment. Higher is this coefficient, faster and more pronunced is the drying of the material with a direct influence on the drying shrinkage strain;
4. analysis of the solid domain influence on the general solution (i.e. case solved by using the pure CFD model).

### *4.1. 10 MW fire ('standard case')*

In this case the total thermal power developed during the fire, is equal to 10 MW which corresponds to a fire due to a burning car. The heat source value increases in 5 min from zero to the maximum value (i.e. 10 MW) and then it can be considered as constant until the final time (10 min). For this analysis 15 300 hexaedral elements are used in the fluid domain, while each cross-section is discretized with 640 quadrilateral elements.

The initial and the boundary conditions selected for this case are:

- For the fluid domain: the atmospheric pressure is imposed at the ends of the tunnel, the initial fluid velocity is equal to zero, close to the tunnel vault the fluid can exchange heat with the concrete structure surface according to the universal profiles ('wall law') described in Section 2.3, Equation (13), with a heat exchange coefficient equal to $\alpha_c = 100\,\mathrm{W/(m^2K)}$. The initial temperature is set to 298.15 for the whole fluid domain.
- For the solid domain: on the inner side of the cross-section, i.e. the vault surface in contact with the fluid, two convective (i.e. Robin) boundary conditions are imposed. The convective heat exchange is governed by the same universal profiles described for the fluid domain with the same exchange coefficient $\alpha_c$. As far as the mass exchange between the surface of concrete and the surrounding environment is concerned, a water vapor pressure equal to 1300 Pa and an exchange coefficient of 0.02 m/s are set. The initial condition for the concrete structure are $p^{\mathrm{g}} = 101325\,\mathrm{Pa}$, $p^{\mathrm{c}} = 7 \times 10^{-7}\,\mathrm{Pa}$, $T = 298.15\,\mathrm{K}$. This set of values corresponds to an initial relative humidity equal to 58%. On the outer side of the cross-sections the values of gas pressure, capillary pressure and temperature are fixed (i.e. Dirichlet bc.s) to the initial ones.

The physical behavior of the fluid is particularly complex. At the beginning of heating, the buoyancy forces lead to an expansion of the fluid with the formation of the related plume. The zones of recirculation create a complex three-dimensional structure. Closer to the heat source a hot air flow moves upward. When this flow reaches the vault of the tunnel, partly propagates in the direction of the openings and partly moves toward the ground close to the source, producing at the same time a cyclical convective motion.

The behavior of the velocity field is represented in Figure 4 at various time instants. Close to the source, due to the flow of ascending air the velocity can reach 7 m/s. The velocity of the air flow moving toward the openings in the upper part of the tunnel, or toward the source in the lower part, is approximately equal to 2 m/s. Two detailed views are shown in Figure 5.

Figure 6 shows the temperature distribution at the same time instants considered for the velocity field. Close to the source, after 10 min of simulation, the fluid reaches a temperature of about 830 K. Close to the tunnel vault the temperature of the air is around 425 K after 2 min and reaches 650 K in 10 min. The graph in Figure 7 describes the distribution of maximum concrete temperature along the longitudinal axis. As expected, the most stressed solid section is the central one, corresponding to the fire location (i.e. the source), at $z = 40\,\mathrm{m}$. The temperature in the solid increases up to 470 K, see Figure 8. The relative humidity distribution shows the typical increase in value due to the so-called 'moisture-clog' that is considered as one of the most important factors for the spalling



DOI: 10.1002/nme

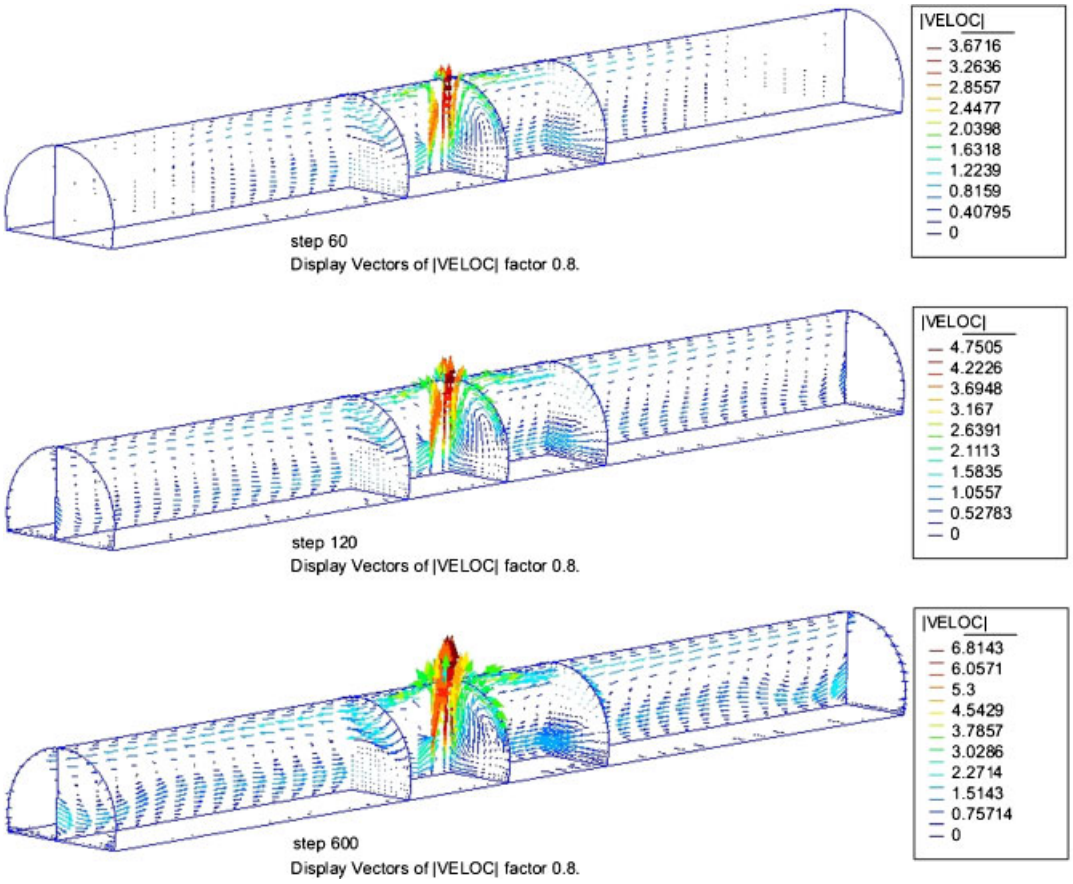


Figure 4. 10 MW case: velocity field (m/s) at $t = 60$, 120, 600 s.

occurrence. In the same zone close to the heated surface of concrete the gas pressure reaches a value of 1 MPa, while the maximum value of total damage is equal to 26%. Considering this situation for the central section, only its external layer it is subjected to a moderate risk of spalling (in particular 'progressive spalling').

### 4.2. *20 MW fire* (*'real case'*)

In this subsection a real fire case is considered. The total thermal power is increasing in 10 min up to 20 MW following a linear law and then kept constant. The geometry, initial conditions and boundary conditions are the same as the previous case of 10 MW, except for the heat exchange coefficient that is now set to $500\,\mathrm{W/(m^2K)}$. The total time of simulation is 1 hour. The case under consideration is more realistic for the total thermal power involved, for the duration of the fire and for the value of the heat exchange coefficient selected. Figure 9 shows that the velocity of the ascensional flux close to the fire source is higher than 9 m/s, while the horizontal fluxes flowing toward the ends of the tunnel have a velocity equal to 3 m/s ($t = 600s$). The temperature distribution in the fluid domain and in the top part of sections S2, S3 (the section of the fire) and S4 are shown in Figures 10–12. The values, both in the fluid and in the solid parts of the tunnel, are higher than those of the case of 10 MW (1216 K instead of 828 in the fluid domain and 659.81 instead 479.15 in the solid sections). In this case the central section, that is the most stressed one, is more exposed to spalling risk. Indeed, the peak of gas pressure (2.4 MPa) in the external layer of the concrete vault (10 cm thick), the formation of the 'moisture-clog' (the relative humidity reaches in this zone a value higher than 90%) and, finally, the total damage ($\backsimeq$55%) can lead to a progressive spalling starting from that layer. Finally, Figure 13 shows the distribution of maximum temperature in the



DOI: 10.1002/nme

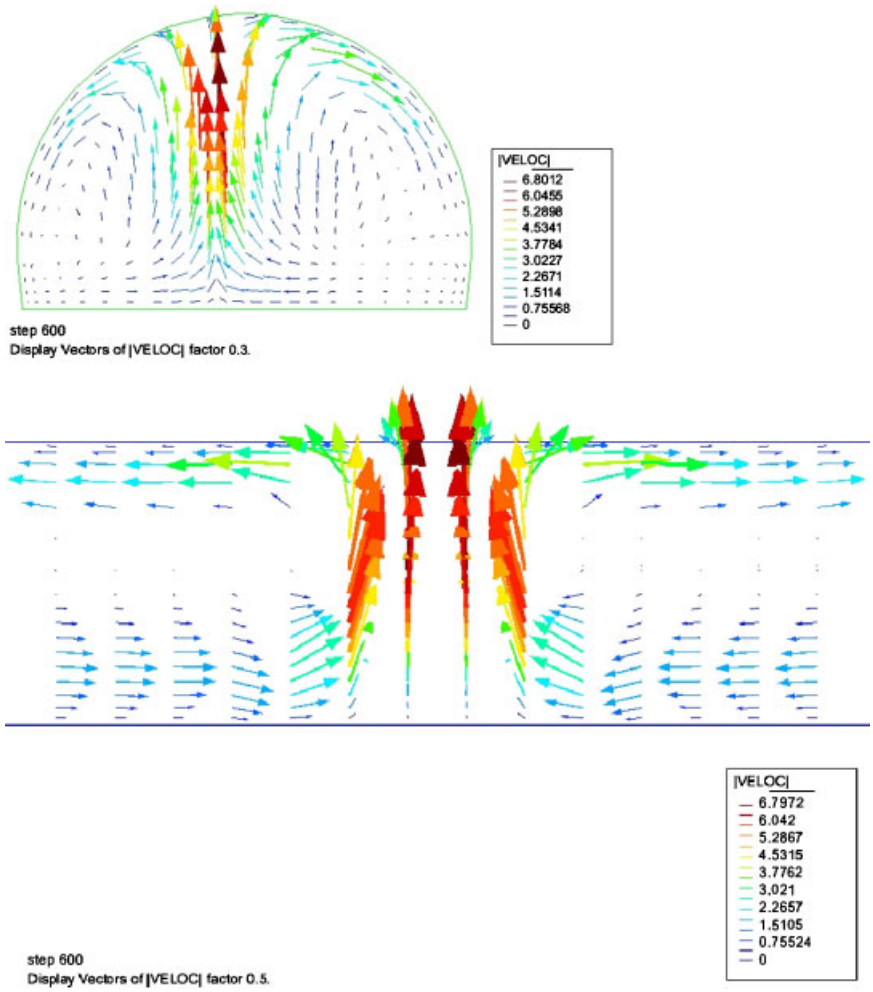


Figure 5. 10 MW case: velocity field (m/s) at $t = 600$ s, cross- and longitudinal-section.

cross-sections along the longitudinal axis and a comparison between the heat source temperature evolution in time and the temperature profiles most used in the literature. The case considered corresponds to a fire with a temperature profile between an ISO-Fire and a Hydro-carbon Fire.

### *4.3. Sensitivity analysis of the heat and mass exchange coefficients*

The zones between the solid and the fluid domain are treated here by using the concept of 'universal profiles' (also known as 'wall law'), see Section 2.3. This means that the heat flux from the environment to the concrete vault is proportional to the temperature difference between the fluid and the solid domain through a parameter that is a sort of heat exchange coefficient, as stated in Equation (13). Higher is this parameter, more the thermal conditions between the domains tend to the 'perfect continuity'. According to the material properties, in the case of concrete tunnel exposed to fire, this coefficient $\alpha_c$ can vary from 100 to 1000 $\mathrm{W/m^2\,K}$. Another important coefficient to take into account is the so-called mass exchange coefficient which governs the water vapor mass exchange between the surface of the concrete structure and the surrounding environment, $\beta_c$. In this subsection we analyze the influence of such parameters on the solution of the coupled problem we are treating, mainly in terms of temperature on the vault surface and capillary pressure which we have chosen as a quantity representative of the hygral state of concrete. The values of the exchange coefficients selected for this sensitivity analysis are: 100 and 500 $\mathrm{W/m^2\,K}$ for $\alpha_c$ and 0.1 and 0.02 m/s for $\beta_c$. Figure 14 shows the evolution of the temperature and capillary pressure



DOI: 10.1002/nme

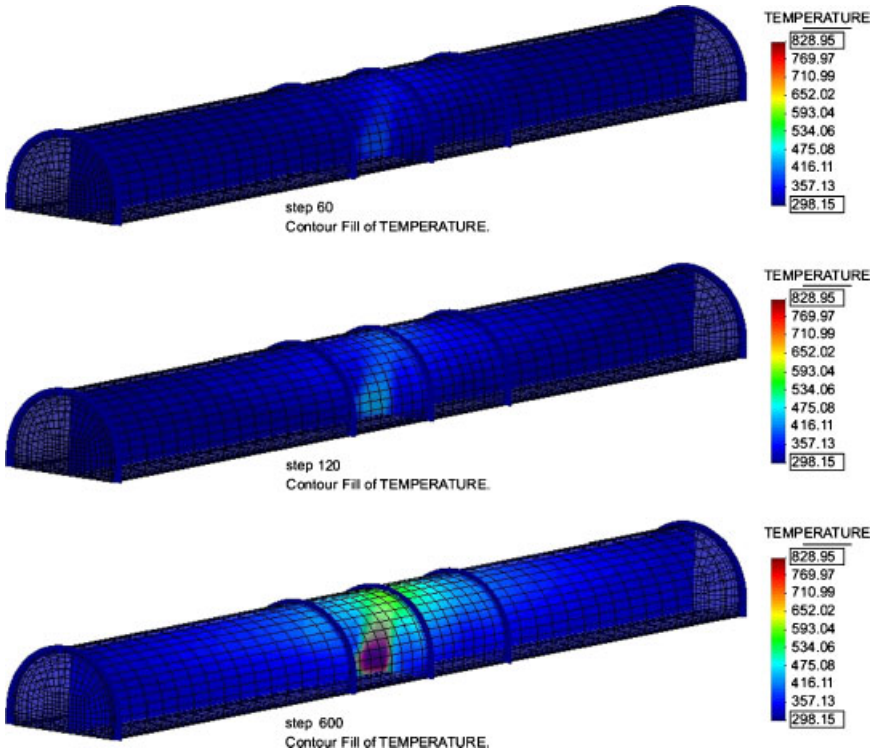


Figure 6. 10 MW case: fluid domain temperature (K) at $t = 60$, 120, 600 s.

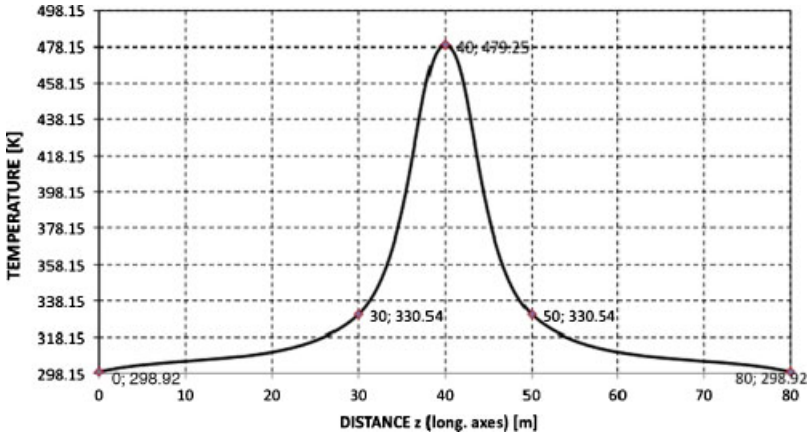


Figure 7. 10 MW case: distribution of the maximum temperature of the cross–sections along the $z$-axis (solid domain).

in a point 2 mm far from the heated surface in the four considered cases. Figure 14(a) shows that there is no influence of the coefficient $\beta_c$ on the temperature evolution (keeping $\alpha_c$ constant), while by varying $\alpha_c$ (and keeping $\beta_c$ constant) the result is rather obvious: higher is the heat exchange coefficient, higher is the surface temperature because of the higher heat flux. However, the differences in terms of temperature tend to decrease in time due to the thermal power that is kept constant after 5 min. The situation is slightly different as far as the hygral state of concrete is concerned. Analyzing the evolution of capillary pressure, we can notice a direct influence of the parameter $\beta_c$ (higher is this parameter, faster is the drying process of concrete on the surface) but



DOI: 10.1002/nme

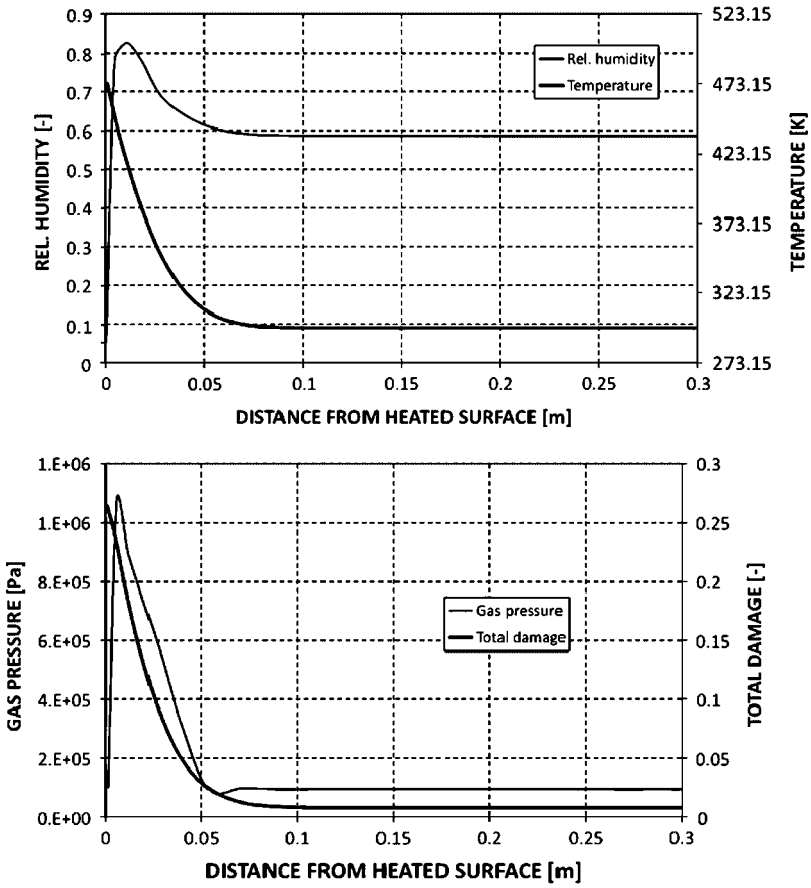


Figure 8. 10 MW case: temperature, relative humidity, gas pressure and total damage distribution along the radial direction on the top of the central cross-section of the tunnel at $t = 10$ min.

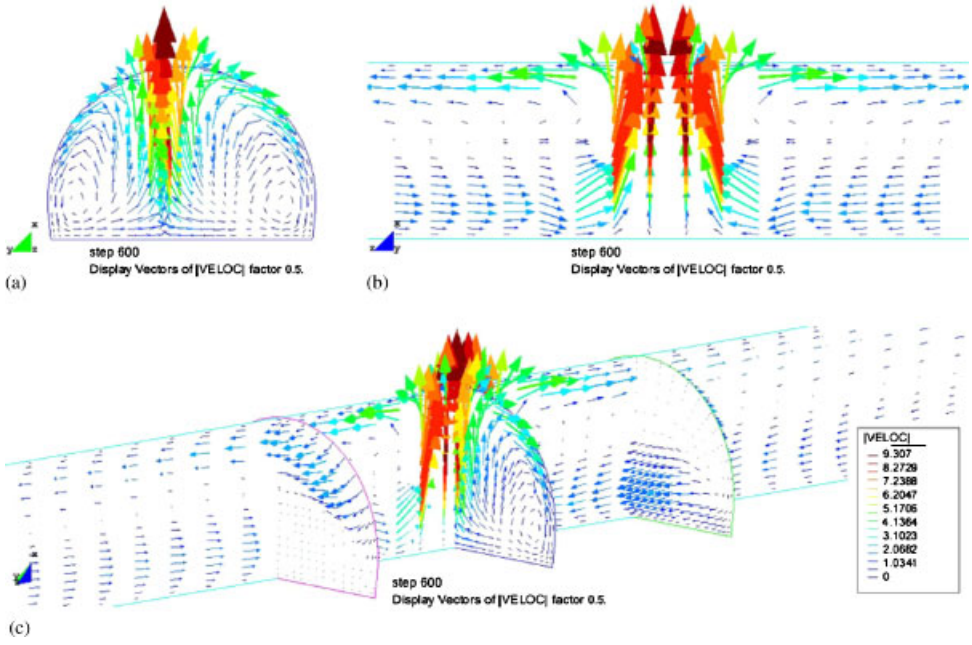


Figure 9. 20 MW case: velocity field (m/s) at $t = 600$ s (c), (a) cross-section and (b) longitudinal section.



DOI: 10.1002/nme

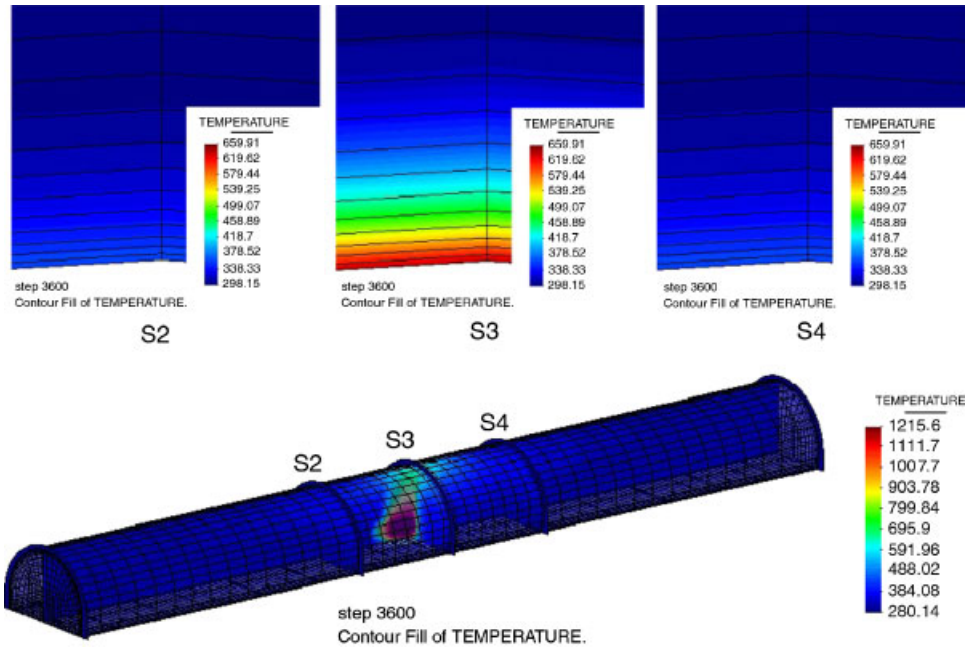


Figure 10. 20 MW: temperature distribution (K) at $t = 3600$ s in the fluid domain and in sections S2, S3 (fire), S4.

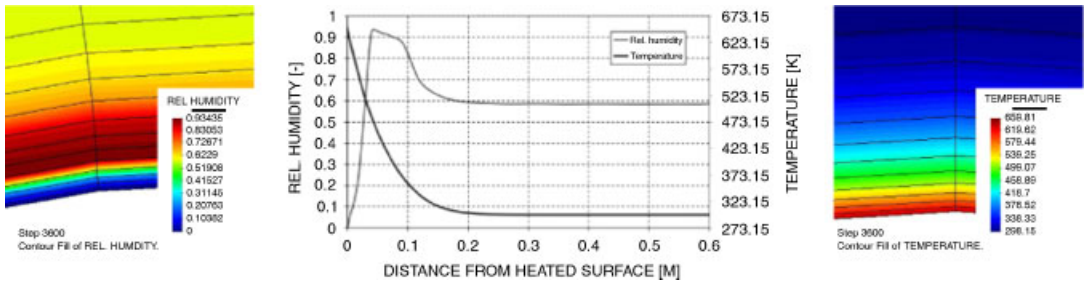


Figure 11. 20 MW case: temperature and relative humidity distribution in the top of the central section S3 (fire) at $t = 3600$ s.

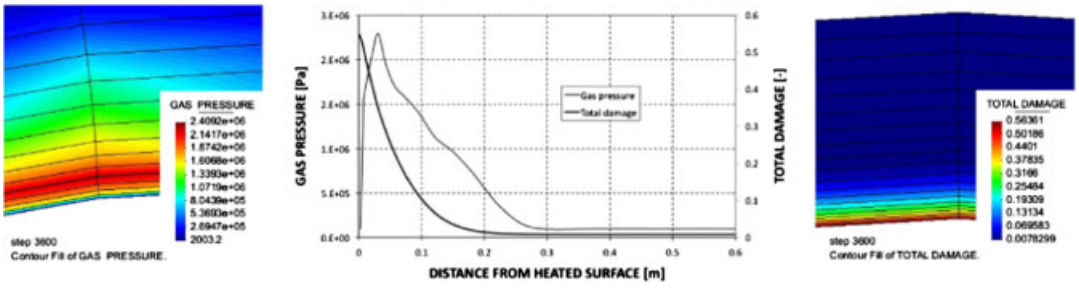


Figure 12. 20 MW case: gas pressure and total damage distribution in the top of the central section S3 (fire) at $t = 3600$ s.

also an indirect influence of $\alpha_c$ (keeping $\beta_c$ constant). This is due to the thermodiffusion process taking place inside the pores of the material: higher $\alpha_c$ means higher heat flux, which lead to a stronger phase change in its pores.



DOI: 10.1002/nme

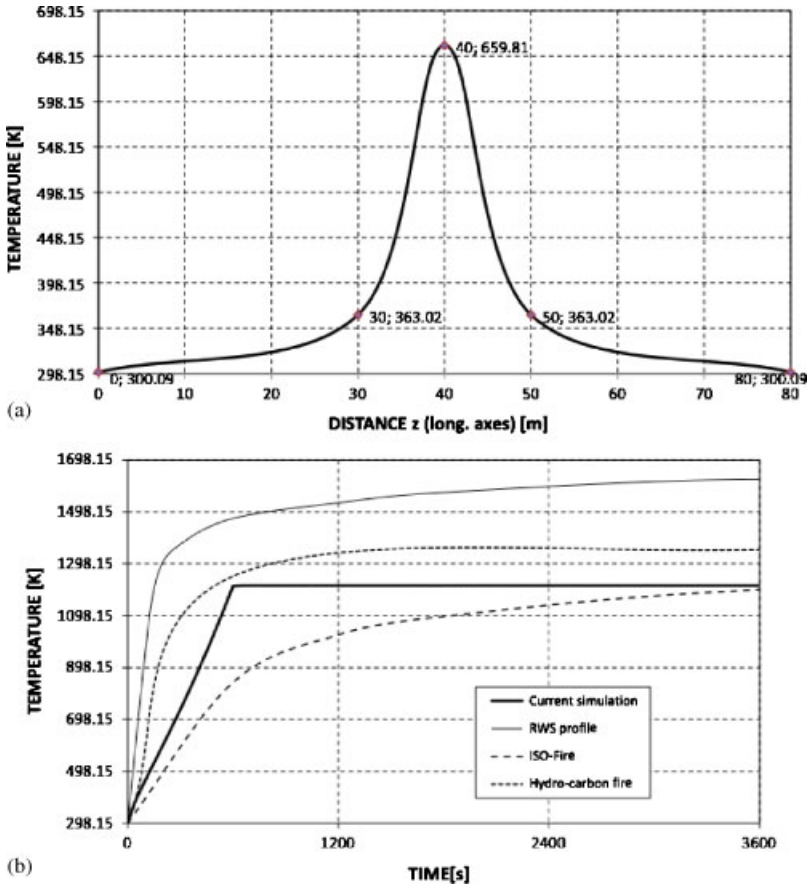


Figure 13. 20 MW case: distribution of the maximum temperature of the cross-sections along the $z$-axis (a) and comparison of the source temperature evolution with the main heating profiles available in the literature.

### *4.4. Analysis of the solid domain influence on the general solution*

In this part the influence of the solid domain on the solution of the coupled problem under consideration is analyzed. The main aim of this calculation is to prove that it is not possible to use a pure CFD code to have an assessment of the temperature field in the layers of fluid in contact with the concrete vault. In this case, the boundary conditions for the thermal field are considered as 'adiabatic'. In Figure 15 the temperature distribution in the fluid domain for both the cases mentioned above (i.e. with and without the solid phase) is shown. Just after 5 min the temperature calculated without considering the concrete vault is much higher than the one obtained by using the fully coupled model, 4230 K vs 753 K. This means that the use of a CFD code solely, leads to an overestimation of the temperature close to the structure, where the values reached are unrealistic. The reader interested to the simplifications that is possible to introduce in the multiphase model for concrete, can refer to [34, 35].

## 5. CONCLUSIONS

A coupling strategy for the simulation of the flow dynamics and structural response of a tunnel in the presence of fire has been developed and presented. Such a kind of model allows for a simulation of fire in tunnels by considering the real fire scenario in a proper way and by taking into account various possible situations (e.g. the actions of fans, firemen, etc.). Moreover, the software



DOI: 10.1002/nme

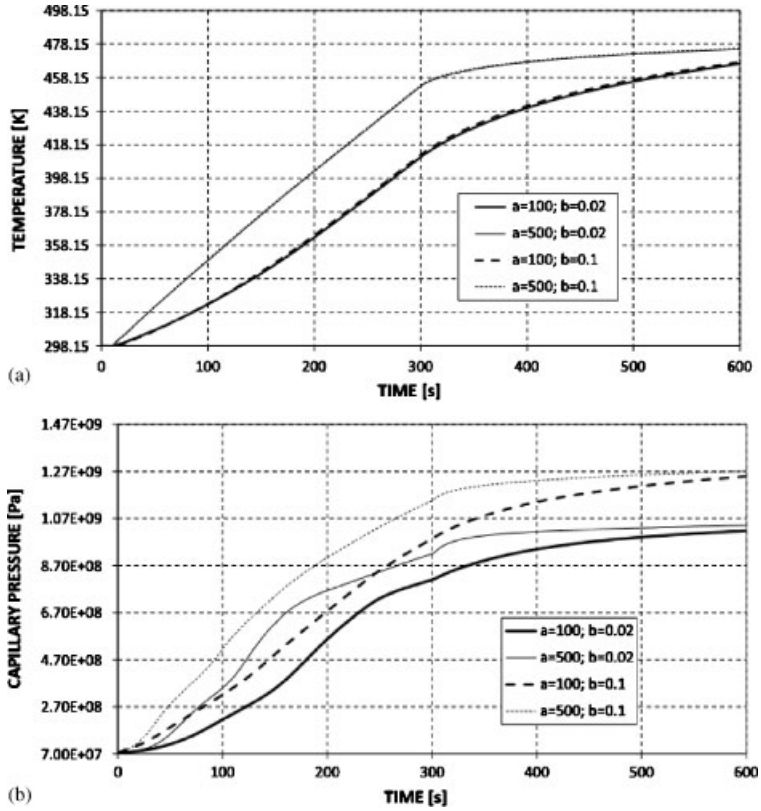


Figure 14. Evolution of temperature (a) and capillary pressure (b) in the top of the vault of the central section for various values of $\alpha_c$ and $\beta_c$ (indicated in the legends as $a$ and $b$).

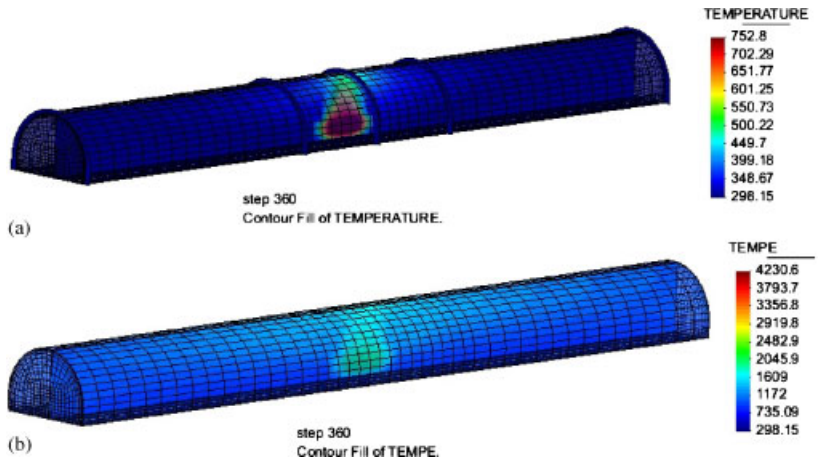


Figure 15. Temperature distribution (K) in the fluid domain in the 'standard case' (a) and in the case without the concrete structure (b) at $t = 5$ min.

tool can be of great practical importance from engineering point of view, for assessing the impact of different scenarios in terms of total thermal power involved, its evolution in time, the position of the source, etc. on the structural response.

From the results obtained in our simulations we can conclude that a fire characterized by a relatively low thermal power (i.e. the 20 MW case) is sufficient to pose the concrete structure at risk, in the central section directly exposed to the fire, at least. This hazard is strictly related to the



DOI: 10.1002/nme

spalling occurrence for the external heated layer of concrete, which can spall off exposing directly the reinforcement bars to the fire action and compromising the structural integrity of the tunnel.

Some points are open to further research. The most important one is the formulation and implementation of a model for the radiation that can be coupled with the CFD and the structural models presented in this work. Indeed, radiation is of importance especially when the fire takes place in an enclosure like for example fire in tunnels. In such a case it is necessary to consider not only the direct radiation, that is the short wave radiation between the fire flames and the surface of the cavity, but also the mutual radiation between different parts of the tunnel vault (i.e. the long wave radiation). Further, for modelling the radiation properly, also smoke radiation and the role played by other participating substances (soot, ash, particle dust, etc.) need to be considered. Such a kind of model for radiation is currently under development.

## ACKNOWLEDGEMENTS

The research was financially supported by the International Centre for Mechanical Sciences 'CISM' in Udine, Italy and the Autostrade del Brennero in Trento, Italy. The authors wish to thank Prof. K. Bergmeister for making the data of the tunnel Virgolo available and Dr. F. Bellinaso for his collaboration. Support from project FITUN, ref. TRA2008-05162, from the Spanish Ministry of Science and Innovation, is also acknowledged.

## REFERENCES

1. Bacchetto A, Principe J, Codina R, Schrefler B. Coupling strategy between a multiphase model for concrete and a stabilized cfd code to simulate the fire effects in tunnels. In *Proceedings of the Conference on Computational Methods for Coupled Problems in Science and Engineering*, Papadrakakis EOM, Schrefler B (eds), Boston, MA, 2005.
2. Eu project uptun—'Cost-effective, sustainable and innovative upgrading methods for fire safety in existing tunnels'. *Technical Report*, UE, 2005.
3. Schrefler BA, Brunello P, Gawin D, Majorana CE, Pesavento F. Concrete at high temperature with application to tunnel fire. *Computation Mechanics* 2002; **29**(1):43–51.
4. Principe J, Codina R. A numerical approximation of the thermal coupling of fluids and solids. *International Journal for Numerical Methods in Fluids* 2009; **59**:1181–1201.
5. Principe J, Codina R. Mathematical models for thermally coupled low speed flows. *Advances in Theoretical and Applied Mechanics* 2009; **2**:93–112.
6. Rehm RG, Baum HR. The equations of motion for thermally driven buoyant flows. *Journal of Research of the National Bureau of Standards* 1978; **83**(3):297–308.
7. Paolucci S. On the filtering of sound from the Navier–Stokes equations. *Technical Report 82-8257*, Sandia National Laboratories, 1982.
8. Majda A, Sethian J. The derivation and numerical solution of the equations for zero Mach number combustion. *Combustion Science and Technology* 1985; **42**:185–205.
9. Sagaut P. *Large Eddy Simulation for Incompressible Flows*. Scientific Computing. Springer: Berlin, 2001.
10. Gawin D, Majorana C, Schrefler B. Numerical analysis of hygro-thermal behaviour and damage of concrete at high temperature. *Mechanics of Cohesive-Frictional Materials* 1999; **4**(1):37–74.
11. Gawin D, Pesavento F, Schrefler B. Modelling of hygro-thermal behaviour of concrete at high temperature with thermo-chemical and mechanical material degradation. *Computer Methods in Applied Mechanics and Engineering* 2003; **192**(13–14):1731–1771.
12. Gawin D, Pesavento F, Schrefler B. Modelling of deformations of high strength concrete at elevated temperatures. *Materials and Structures* 2004; **37**(268):218–236.
13. Gawin D, Pesavento F, Schrefler B. Towards prediction of the thermal spalling risk through a multi-phase porous media model of concrete. *Computer Methods in Applied Mechanics and Engineering* 2006; **20**(4): 5707–5729.
14. Gawin D, Pesavento F, Schrefler BA. Modelling of hygro-thermal behaviour and damage of concrete at temperature above the critical point of water. *International Journal for Numerical and Analytical Methods in Geomechanics* 2002; **26**(6):537–562.
15. Gray W, Schrefler B. Thermodynamic approach to effective stress in partially saturated porous media. *European Journal of Mechanics/A Solids* 2001; 521–538.
16. Gray W, Schrefler B. Analysis of the solid phase stress tensor in multiphase porous media. *International Journal for Numerical and Analytical Methods in Geomechanics* 2007; **31**(4):541–581.
17. Pesavento F, Gawin D, Schrefler BA. Modeling cementitious materials as multiphase porous media: theoretical framework and applications. *Acta Mechanica* 2008; **201**(1–4):313–339.



DOI: 10.1002/nme

18. Gray W, Schrefler BA, Pesavento F. The solid phase stress tensor in porous media mechanics and the hill-mandel condition. *Journal of the Mechanics and Physics of Solids* 2009; **57**:539–554.
19. Mazars J. Application de la mecanique de l' endommagement au comportament non-lineaire et la rupture du beton de structure. *Ph.D. Thesis*, L.M.T., Universite de Paris, France, 1984.
20. Pijaudier-Cabot J. Continuum models for materials with microstructure. *Non-Local Damage*, Chapter 4. Wiley: Chichester, 1995; 105–143.
21. Lewis RW, Schrefler BA. *The Finite Element Method in the Static and Dynamic Deformation and Consolidation of Porous Media*. Wiley: Chichester, 1998.
22. Gawin D, Pesavento F, Schrefler BA. Modelling creep and shrinkage of concrete by means of effective stresses. *Materials and Structures* 2007; **40**(6):579–591.
23. Khoury GA. Strain components of nuclear-reactor concretes during first heat cycle. *Nuclear Engineering and Design* 1995; **156**(1–2):313–321.
24. Thelandersson S. Modeling of combined thermal and mechanical action on concrete. *Journal of Engineering Mechanics* (ASCE) 1987; **113**(6):893–906.
25. Witek A, Gawin D, Pesavento F, Schrefler B. Finite element analysis of various methods for protection of concrete structures against spalling during fire. *Computation Mechanics* 2007; **39**(3):271–292.
26. Principe J, Codina R. A stabilized finite element approximation of low speed thermally coupled flows. *International Journal of Numerical Methods for Heat and Fluid Flow* 2009; **18**(7/8):835–867.
27. Codina R. Stabilization of incompressibility and convection through orthogonal sub-scales in finite element methods. *Computer Methods in Applied Mechanics and Engineering* 2000; **190**(13–14):1579–1599.
28. Codina R. On stabilized finite element methods for linear systems of convection–diffusion–reaction equations. *Computer Methods in Applied Mechanics and Engineering* 2000; **188**(1–3):61–82.
29. Hughes RTJ. Multiscale phenomena, Green's functions, the Dirichlet-to-Neuman formulation, subgrid scale models, bubbles and the origins of stabilized methods. *Computer Methods in Applied Mechanics and Engineering* 1995; **127**:387–401.
30. Codina R. Stabilized finite element approximation of transient incompressible flows using orthogonal subscales. *Computer Methods in Applied Mechanics and Engineering* 2002; **191**(39–40):4295–4321.
31. Principe J, Codina R, Henke F. The dissipative structure of variational multiscale methods for incompressible flows. *Computer Methods in Applied Mechanics and Engineering* 2010; **199**:791–801.
32. Zienkiewicz ORTC. *The Finite Element Method*: *The Basis*, vol. 1. Butterworth-Heinemann: Oxford, 2000.
33. Pesavento F. Non-linear modelling of concrete as multiphase porous material in high temperature conditions. *Ph.D. Thesis*, Department of Structural and Transportation Engineering, University of Padova, 2000.
34. Gawin D, Pesavento F, Schrefler BA. What physical phenomena can be neglected when modelling concrete at high temperature? a comparative study. Part 1: physical phenomena and mathematical model. *International Journal of Solids and Structures*, in print.
35. Gawin D, Pesavento F, Schrefler BA. What physical phenomena can be neglected when modelling concrete at high temperature? A comparative study. Part 2: comparison between models. *International Journal of Solids and Structures*, in print.



DOI: 10.1002/nme